Surface engineering of ultra-hard polycrystalline structures using a nanosecond Yb fibre laser: Effect of process parameters on microstructure, hardness and surface finish

PLEASE CITE THE PUBLISHED VERSION

https://doi.org/10.1016/j.jmatprotec.2018.11.014

PUBLISHER

© Elsevier

VERSION

AM (Accepted Manuscript)

PUBLISHER STATEMENT

This paper was accepted for publication in the journal Journal of Materials Processing Technology and the definitive published version is available at https://doi.org/10.1016/j.jmatprotec.2018.11.014

REPOSITORY RECORD

Pacella, Manuela, Vahid Nekouie, and Amir Badiee. 2018. “Surface Engineering of Ultra-hard Polycrystalline Structures Using a Nanosecond Yb Fibre Laser: Effect of Process Parameters on Microstructure, Hardness and Surface Finish”. figshare. https://hdl.handle.net/2134/36217.

Surface engineering of ultra-hard polycrystalline structures using a Nanosecond Yb fibre laser: effect of process parameters on microstructure, hardness and surface finish.

Manuela Pacella [a,*], Vahid Nekouie [b], Amir Badiee [c]

[a] Wolfson School of Mechanical, Electrical and Manufacturing Engineering, Loughborough University, Loughborough, Leicestershire, LE11 3TU, UK

[b] Royce Research Centre, Materials Science and Engineering, The University of Sheffield, Western Bank, Sheffield, S10 2TN, UK

[c] School of Engineering, College of Science, University of Lincoln, Lincolnshire, LN6 7TS, UK

Abstract

The use of lasers for near-net shape manufacturing of cutting tools, made of ultra-hard materials such as polycrystalline diamonds, is recently becoming a standard processing step for cutting tool manufacturers. Due to the different machinability exhibited by microstructurally different composites, the laser processing parameters and their effects need to be investigated systematically when changing the material. In this context, the present paper investigates the effects of a fibre laser milling process (nanosecond pulse duration) on surface topography, roughness, microstructure and microhardness of two microstructurally different polycrystalline diamond composites. Pockets were first milled using a pulsed ytterbium-doped fibre laser (1064 nm wavelength) at different fluences, feed speeds and pulse durations, and finally characterised using a combination of Scanning Electron Microscopy, White Light Interferometry, Energy Dispersive using X-Ray (EDX) and micro hardness analyses. For laser feed speed in the region of 1000 mm/s, micro-indentation tests revealed an improvement of hardness from 75 GPa to 240 GPa at a depth of 350nm, and to 258 GPa at a depth of 650nm below which the microstructure is preserved as confirmed by microscopy images of the analysed cross sections. For fluences in the region of 11.34 Jcm^{-2} a variation of cobalt binder volume between the two composites causes a change in milling mechanism. At fluences below 20 Jcm^{-2}, the proposed milling process for CTM302 resulted in a microstructural change (ultra-hard grain size and Cobalt binder weight), better surface integrity (140 nm) and improvement of micro hardness (up to 258 GPa). The properties achieved through the proposed process achieve better hardness and roughness when compared to laser shock processing. To the best of authors' knowledge, it is reported for the first time that an increase of hardness accompanied by improved surface roughness can be achieved on polycrystalline diamond through low-energy laser processing.

Keywords

Polycrystalline diamond

Laser milling

Nanosecond Ytterbium fibre laser

Laser shock processing

Microstructure change

1. Introduction

Polycrystalline diamond (PCD) materials are used in a wide range of industrial applications, from oil and gas exploitation where they are employed for drill bits, to mining, drilling and road planing. However, the fastest growing market for these materials resides in the cutting tool industry where PCDs are employed to machine complex automotive and aerospace components. Efficiency and productivity in precision machining industries are to be prioritized due to the large quantity of components manufactured daily.

PCD grades are highly suitable for defined edge cutting tool applications considering their high thermal conductivity at room temperature, 325–550 W m^{-1} K^{-1} (Kidalov and Shakov (2009)), and their exceptional micro-hardness of 48–52 GPa (Cook and Bossom, (2000)). Some of the common applications include machining of non-ferrous materials, such as high-silicon aluminium, metal matrix composites and carbon fibre reinforced plastics. The same properties which make PCD the hardest synthetic material, also classify them as difficult to cut materials. This justify the need of looking at unconventional technology for engraving, shaping and micro design diamond surfaces to increase productivity and reduce manufacturing costs.

Common industrial technologies for the manufacture of diamond cutting tools are mechanical grinding and electrical discharge machining (EDM). The former technology is performed using diamond abrasives wheels; however, this introduces undesirable microcracks into the workpiece due to the diamond crystals bonded in cobalt, thus the abrasive tool can excise individual grains, leaving voids. At the same time Brecher et al.

(2013) reported that grinding is costly due to low material removal rates and high wear of the grinding wheel, thus it is relatively inefficient. Micro wire-EDM has emerged as a fast, economic and precise way to micro-machine electrically conductive PCD blanks. Cobalt present in the matrix in the form of a binder makes the composite electrically conductive. However, Yan et al. (2013) reported that because the wire cannot cut through the diamond grains and depending on the level of thermal damage suffered by the electrode, thermal damage on the machined surface of PCD is unavoidable after wire-EDM. As a consequence poor surface finish with the increased grain sizes is inevitable due to the grain breakouts and voids.

Since geometrical accuracy and surface integrity (surface roughness, damaged layer, and surface quality) have great influence on cutting tool life, common industrial practise is to wire-EDM cut of the PCD blanks and subsequently to electrically discharge grind (EDG) the cutting edge to produce the desired edge geometry and roughness. In this context, laser processing offers a versatile approach which proved to be applicable to difficult-to cut ultra-hard materials, as firstly reported by Dold et al. (2012-2013) and later investigated by previous research from Pacella et al. (2014-2015).

Using high intensity pulsed visible laser radiation, this technology ablates diamond materials via a thermal process with high efficiency, high flexibility and small (nanometric) sub-surface damage when the process is optimised, as demonstrated by Butler-Smith et al. (2013) and Pacella et al. (2014). Recent developments of laser systems show a significant interest for fibre lasers making them the preferred option to the Q-switched diode-pumped solid-state (DPSS) systems. Some of the advantages of the fibre laser systems reside in the flexibility of operating window in terms of repetition rate, pulse shape, duration and lower costs. Numerous studies are reported on the use of pulsed neodymium-doped yttrium aluminium garnet (Nd: YAG) lasers to process ultra-hard materials, with emphasis on the effect of laser conditions on the material topography and surface integrity post-processing. The effect of change in laser output power, repetition frequency, pulse duration and feed speed on the chemical composition of a coarse and fine grained PCD were investigated by Pacella et al. (2014). Experimental findings revealed an increase of cobalt proportional to the laser energy density, showing a relation between laser energy distribution and extent of material chemical modification. Pacella et al. (2014) investigated the surface integrity of PCD structures after processing with a microsecond Nd:YAG laser via a combination of focused ion beam milling and high resolution transmission electron microscopy. This revealed amorphous carbon and graphitic structures formed after the ablation process and an undisturbed PCD composite substructure below the graphitic boundary. The examination of local high and low laser fluence ablated sites showed that the extent of residual deposits (amorphic and graphitic carbon) is related to the level of fluence during ablation. Pacella et al. (2015) also reported that, since cobalt is embedded in the diamond matrix, because of a difference in thermal conductivity between diamond grains and binder, important phenomena of expansion and compression between diamond and cobalt take place during the ablation process, which are also dependent on the energy density involved in laser processing.

Brecher et al. (2013) studied the effects of a two-step process technique (laser and grinding) in precision finishing of a 10 µm sized diamond grains PCD cutting tool. In this case a neodymium-doped yttrium orthovanadate (Nd: YVO4) laser was used after dicing and prior grinding to remove the surface layer of the cutting edge promoting improved surface finish, reduced time for manufacture and improving grinding wheel wear resistance. This work found a linear relationship between applied laser fluence and the absolute ablation and no debris due to melt expulsion (which is typical for short pulse laser ablation) was found. Dold et al. (2013) focussed on the manufacture of cutting edges in PCD turning inserts using a picosecond master oscillator power amplified (MOPA) laser source. Experiments were carried out on two different grained PCD structures: fine (average ultra-hard grain size = 2-4 µm) and coarse (average ultra-hard grain size = 25 µm). Improved wear resistance and tool lifetime were found in the tools processed by laser. In addition to these works, Wu et al. (2014) investigated the formation mechanism of polycrystalline diamond surfaces milled by a nanosecond pulsed fibre laser and the effect of process parameters on material removal rate and surface roughness. The main findings of the study were that pulse energy and pulse overlap have a significant effect on the milled surface morphology, that optimum pulse overlap with moderate pulse energy may be used; and that a good compromise of surface quality and productivity can be achieved when scan overlap is selected near its optimum value at around 50%. Deng and Molian (2012) investigated the effect of laser shock wave treatment on a polycrystalline diamond tool with a grain size of 10 µm and cobalt binder of 10 % volume, focusing on laser induced phase transition and hardness change. Main claim was that pulse repetition rate was more sensitive than peak power density in producing a change of hardness, due to an increased dislocation density. However, an increased in surface roughness and a reduction of surface integrity were also reported.

The main conclusion that can be drawn from previous works in this area is that numerous laser parameters might affect the laser micro-machining of ultra-hard composite structures. However, most published studies focused on laser milling methodologies on a specific grade of PCD materials, with no focus on the understanding of the role played by the binder and its thermo-mechanical properties, which noticeably differ from the ultra-hard diamond grains. No attention has been given to the importance of the ultra-hard grain size and binder composition and their different thermal reaction to the laser milling process. In addition to this, limited research has been carried out in the use of MOPA-based Yb fibre laser systems for milling microstructurally different PCDs. The viability of this technology in achieving an improvement in material properties (e.g. hardness) and for micro-engineering the ultra-hard materials has not been investigated.

1.1 Scope of the paper

In the need to increase the productivity of ultra-hard materials manufacture, enhance process reliability, and improve the performances of cutting tool materials in real machining applications, the objectives of the proposed research are threefold. Firstly, using a pulsed ytterbium-doped fibre laser (1,064-nm wavelength, 20W maximum output power) an experimental study is proposed to investigate the effect of programmable parameters and energetic conditions in the processing of two microscopically different PCD materials and introduce alternative technique to achieve polished multi-modal PCD structures. Secondly, an evaluation of the role of binder volume and hard grain size in fibre laser milling of PCDs is conducted via topographical, microscopical and micro-indentation tests and a new set of laser operating conditions is proposed to enhance the micro-hardness of these materials. Thirdly, an in-depth analysis of the effect of each laser parameter is conducted on two microstructurally different PCD materials to provide a fundamental understanding of the role of binder in the thermal/ablative mechanism for ultra-hard composites, thus establishing the basis for laser surface engineering the microstructure of PCDs.

2. Methodology

2.1 Materials

Two microstructurally different commercially available PCD materials (0.5 mm diamond layer) directly synthetized on a tungsten carbide substrate were selected for this study: CTB010, a medium grain composite with an average diamond grain size of 10 µm and CTM302, a multi-modal grain composite with average diamond grain size of 2-30 µm infiltrated by cobalt as metallic binder (Co binder volume circa 12% and 10% respectively) supplied by Element Six Ltd. The main difference between the commercially available PCD composites (Figure 1) is the grain size, which considering the extent of crystallographic intergrowth, will affect also the cobalt binder volume. The reason for analysing both the average diamond grain size of 10 µm and the multi-modal one resides in the importance to deeply understand the role of binder in the ablation process to enable this technology to be efficiently included in the industrial processing of ultra-hard cutting tools.

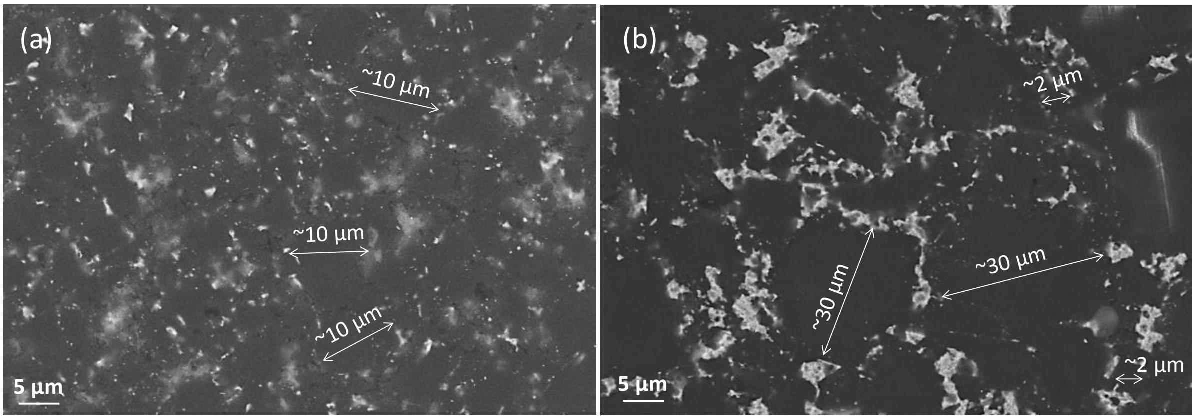

Figure 1: SEM micrographs before machining of a) CTB010 and b) CTM302.

Both grades, in fact are used for precision machining of various components and in different applications. Cook and Bossom (2000) reported that CTB010 is commonly used when roughing and finishing characteristics are needed in a single tool, due to its balance of wear resistance and toughness. CTM302 is mostly used when edge strength and edge quality are required, thanks to its good thermal stability in applications and good abrasion resistance. The thermal properties of diamond and Cobalt are presented in Table 1.

Table 1. Material properties from Zaitsev (2001).

Properties	Diamond	Cobalt
Density (kg m^{-3})	4000	20.432T + 8994.3 (solid) 7760 - 1.09 (T-T_{mCo}) (liquid)
Enthalpy (kJ mol^{-1})	710.9	382.4
Melting temperature (K)	/	1768
Graphitisation temperature (K)	1050	/
Vaporisation temperature (K)	4827	3200
Thermal conductivity (W m^{-1} K^{-1})	540	-0.0367T + 94.2 (solid) 21.5 + 0.0082T (liquid)
Specific heat at constant pressure (J kg^{-1} K^{-1})	516 (300 K), 2058 (1800 K), 2192 (3000 K)	0.22T + 380.06 (solid) 685.9 (liquid)
Thermal expansion coefficient (10^{-6} K^{-1})	3.8	12.2

2.2 Laser machining technique

A 20 W single mode SPI pulsed Yb-doped fibre laser (1064 nm wavelength) based on a MOPA amplifier was used to process the samples. This is based on a tuning technology of delivered pulses based on direct modulation of the seed laser allowing programmed waveforms. The waveforms are the results of an optimization of the peak power at a specific pulse repetition rate. Two waveforms were considered for the experiments: waveform 0 (repetition rate at which the peak power is optimised, 35 kHz; pulse duration 220 ns; maximum pulse energy, 0.57 mJ) and waveform 24 (repetition rate at which the peak power is optimised, 105 kHz; pulse duration 45 ns; maximum pulse energy, 0.19 mJ). Laser parameters and ranges for the experiments are reported in Table 2.

Table 2. Machining parameter range.

Process parameters	Range of values	Fit screening model design
Intensity I (%)	80-100	80, 100

Repetition frequency f (kHz)	35-105	35, 105
Feed speed FS (mm s^{-1})	70-1000	400, 1000
Number of passes N	1-5	1, 5
Depth of cut doc (μm)	1-5	1, 5
Track distance TD (μm)	20-28	20, 28
Pocket Size (mm^2)	1	1
Pulse duration τ (ns)	45-220	45, 220
Fluence ψ (J cm^{-2})	3.78-11.34	3.78, 11.34

All laser processing experiments performed in this study were conducted in ambient air. A touch probe was used to optimize the focal distance and programmable set-up utilised to machine a pocket with area of 1 mm^2. A focus spot diameter of size 40 μm was used, and the generated laser fluence was calculated based on previous research from Pacella et al. (2014). Initially, a fit screening experimental design was run (Table 2) for the identification of the main affecting processing parameters on the topography and microstructure. This consisted of 6 factors each at 2 levels, resulting in 12 experimental conditions. This set of 12 experiments was repeated 3 times to increase its robustness.

The second experiment focused on developing a fundamental understanding of the complex thermo-mechanical phenomena occurring at low laser feed speeds, with attention to the surface roughness, micro hardness and microstructural characteristics in the laser processed regions. The selected factors (variables) were feed speed and track distance; each at three levels, the values chosen for each parameter level are provided in Table 3. This resulted in a Taguchi L6 orthogonal array. This set of 6 experiment was repeated 3 times to increase its robustness. Feed was varied between 70 and 350 mms^{-1} (I = 100%, τ = 220 ns, ψ = 11.34 J cm^{-2}). Feed speed values resulted in theoretical overlapping values of the beam area spots of 75% (for a feed speed of 350 mm s^{-1}), 80% (280 mm s^{-1}), 85% (210 mm s^{-1}), 90% (140 mm s^{-1}) and 95% (70 mm s^{-1}) respectively, calculated based on previous research from Dahotre and Harimkar (2008).

Table 3. Parameter values at each level.

Parameter	Code	Level 1	Level 2	Level 3
Track distance (μm)	A	20	24	28
Feed speed (mm s^{-1})	B	70	210	350

2.3 Material characterisation method

All test specimens were cleaned in an ultrasonic bath for 20 minutes after laser machining to remove any debris or deposition due to the processing. The depth and diameter of the machined craters were measured using a White Light Interferometer (WLI-MicroXAM ADE Phase Shift), while topographical characterisation and Energy Dispersive Spectroscopy (EDS) analyses were achieved using a Scanning Electron Microscope SEM (XB1540 Carl Zeiss). Surface roughness measurements including Ra, Rz and Rt were achieved for all the processed samples using a Talysurf Series 2 (Taylor/Hobson). Based on research by Bitelli et al (2012) Ra is the more representative parameter of the roughness, however for a smaller set of specimens which required a more in-depth analysis, a high-resolution optical 3D measurement system Alicona InfiniteFocus was used. Each laser processed sample was scanned, and three single profiles were extracted from top, bottom and centre of each area. For each sample, three Abbott-Firestone’s curves were plotted based on ISO 13565, and their respective 2D roughness parameters Rk, Rpk and Rvk extrapolated from each curve. Their 3D counterparts namely Sk, Spk and Svk were derived based on ISO 25178 from the Abbott-Firestone’s curve relative to the entire surface.

Indentation tests were conducted with a NanoTest system (Micro Materials Ltd.) equipped with a Vickers indenter. All hardness tests on polycrystalline diamond specimens were performed at room temperature (23°C) and controlled load. A holding (dwell) time was set 30 s to allow negligible creep displacement. A thermal shift correction was used so that absolute values of a thermal drift rate were usually well below 0.05 nm s^{-1}. During the indentation test, a maximum load of 500 mN was applied on the as-received and processed samples. A loading rate of 3 mN s^{-1} was used to investigate the hardness variation. In addition to this, incremental loading-unloading test were performed to measure the hardness values at different indentation depths at the same location in the specimen. These experiments were performed using the Vickers tip in the load range 500-2500 mN with a constant loading rate of 3 mN s^{-1}. Unloading was performed with a rate of 6 mN s^{-1} down to a prescribed limit of 20% of the load peak in the previous cycle. The micro hardness was measured only for selected processing conditions and for CTM302 due to the high surface quality results and the possibility of using these conditions for precision finishing applications. Processing conditions for which micro-hardness values have been measured are shown in Table 4.

Table 4. Processing parameters for micro-hardness measurements.

Test	I	Wave	f	FS	N	doc	TD
B5	100	0	35	210	1	5	28
D4	80	24	105	1000	5	5	28
D5	100	24	105	1000	1	1	20
D6	100	0	35	350	1	5	20
C1	100	0	35	70	1	5	22
C2	100	24	105	1000	5	1	20
C7	100	0	35	400	5	1	28
C5	80	0	35	1000	5	1	28
E4	100	0	35	350	1	5	20
E5	100	0	35	210	1	5	24
C2	100	24	105	1000	5	1	20
C3	100	0	35	1000	1	5	28
C4	80	0	35	1000	1	5	20

3. Results and discussion

3.1 Effect of laser feed speed on the machining mechanism

The first experimental study investigated the effect of laser feed speed on surface roughness and topographical profile of the milled pockets. Average surface roughness Ra of the as-received samples based on 5 measurements was 90.1 nm for CTM302 and 66.5 nm for CTB010 respectively. 2D parameters Rk, Rpk and Rvk were 0.255 µm, 0.128 µm, 0.161 µm for CTM302 and 0.181 µm, 0.156 µm, 0.097 µm for CTB010. 3D surface parameters Sk, Spk, Svk were 0.294 µm, 0.154 µm, 0.241 µm for CTM302 and 0.219 µm, 0.333 µm and 0.132 µm for CTB010 respectively. An example of an extracted Abbott-Firestone's for the as-received materials CTM302 and CTB010 is shown in Figures 2b, d. 3D texture measurements proved CTM302 to have higher core surface roughness Sk, however lower Spk (average height of the protruding peaks above the core surface profile). Spk also represents the ability of a surface to resist wear, thus, the smaller Spk, the higher the wear resistance. Spk for the as-received CTB010 was twice greater than Spk for CTM302, this is expected due to the microstructural difference between the two materials and the higher Cobalt presence in CTB010.

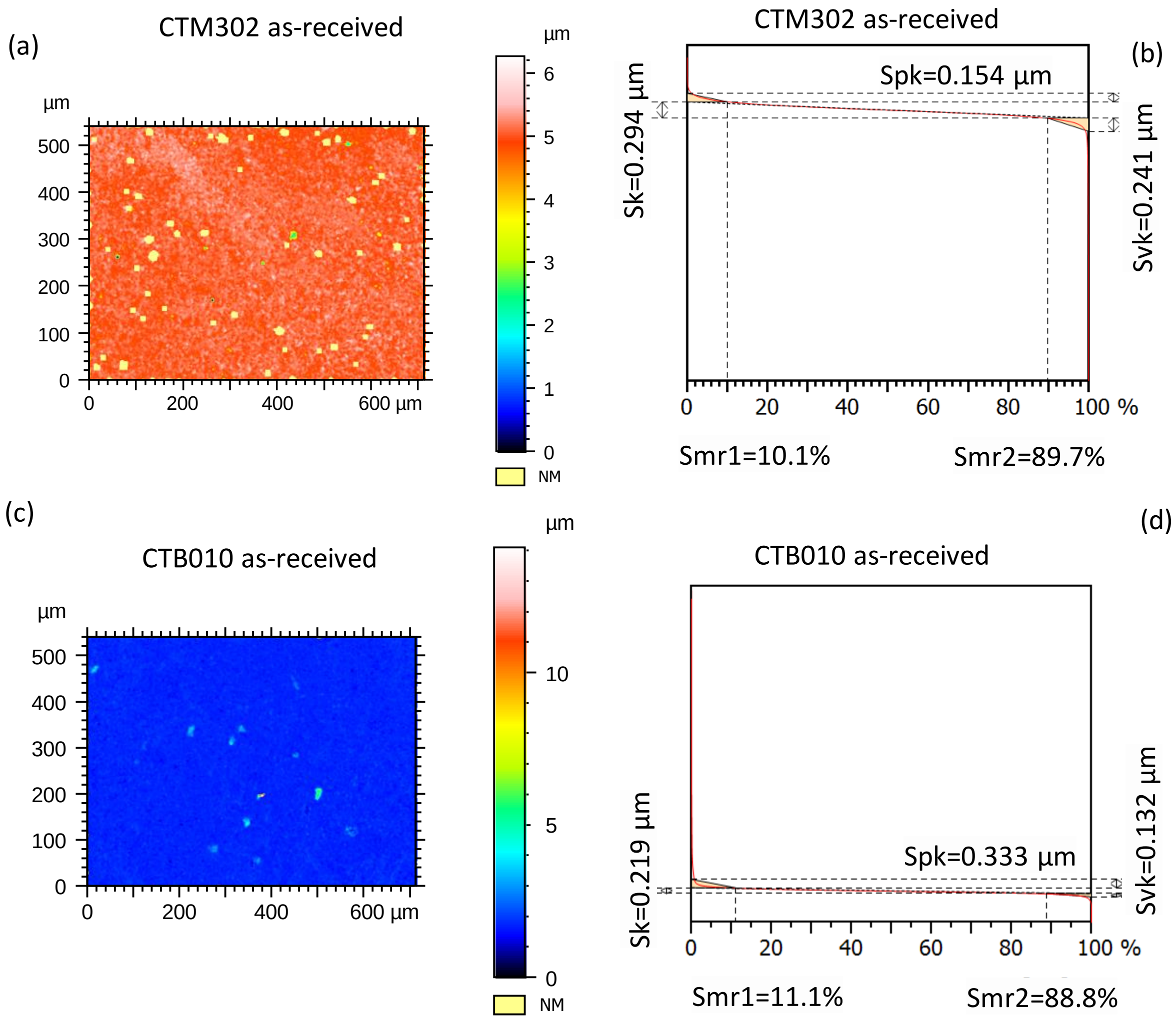

Figure 2: Abbott curve for one as-received surface and parameters Sk, Spk, Svk for two microscopically different materials.

Feed speed variation showed to noticeably affect the achieved surface roughness, as represented in Figure 3, where a wider variation between minimum and maximum values in the boxplots indicate a higher dependence of two-dimensional roughness parameters from laser feed speed for that specific material. CTB010 textures were significantly affected by laser feed speed as evidenced by the variation between first and third quartile in all the boxplots in Figure 3 a-d. A different result was achieved for CTM302 where a change of feed speed altered only the average height of the protruding peaks above the core profile Rpk (Figure 3c) and its 3D counterpart Spk (Figure 3c). In all results for CTB010 and for CTM302, Spk values are below 1 µm, however the measured values at different feed speeds are higher than the as-received samples. This provides a valuable tool for engineering the wear properties of polycrystalline materials trough laser processing.

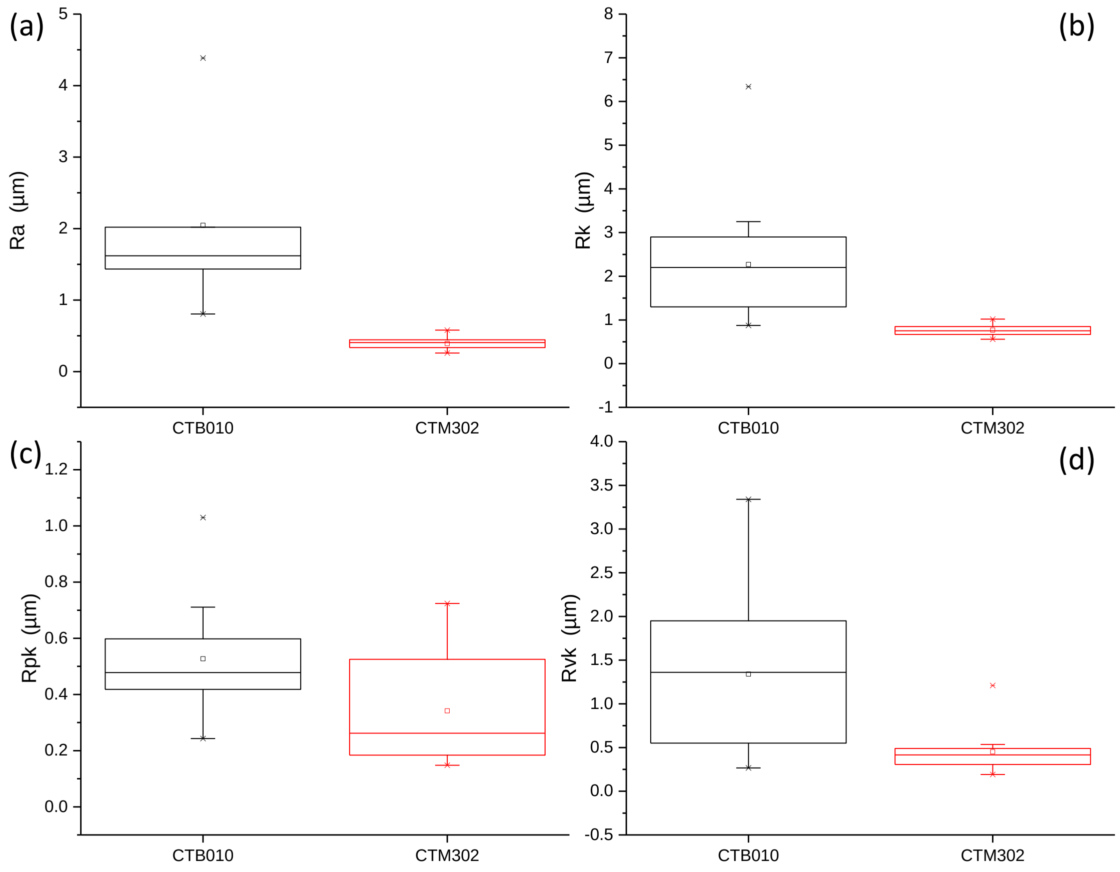

Figure 3: Effect of feed speed on 2D surface roughness parameters for the two microscopically different materials.

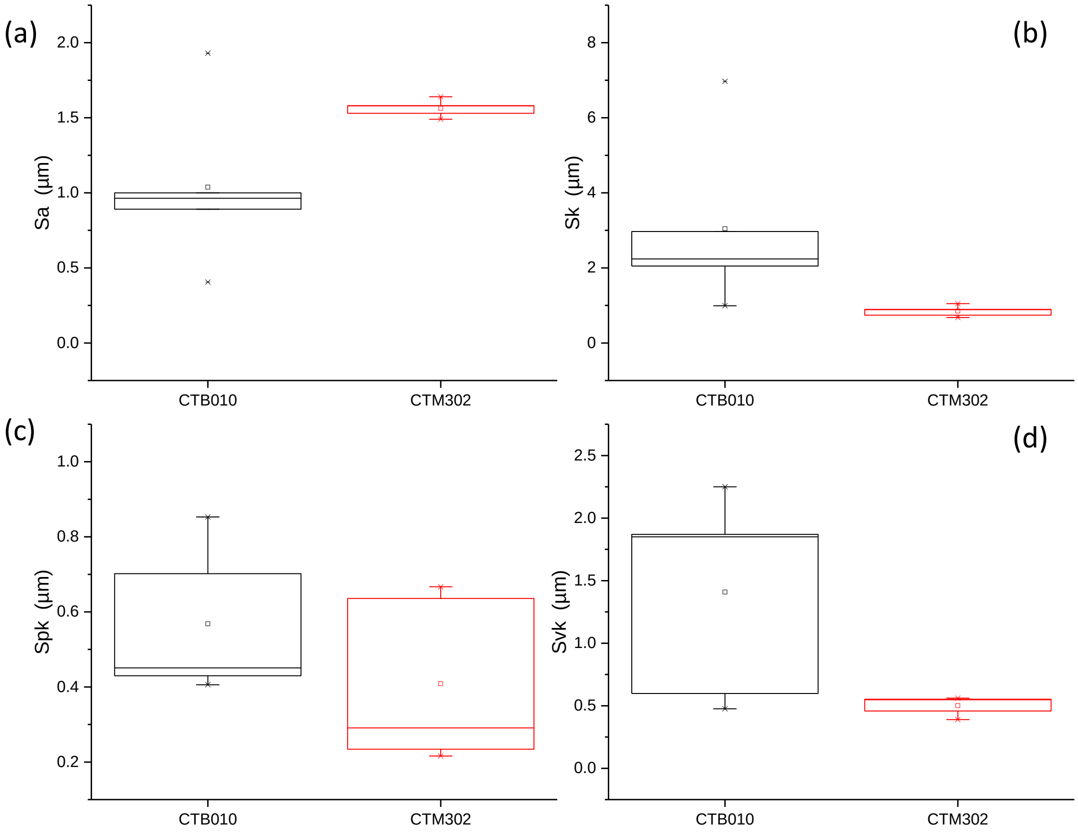

Figure 4: Effect of feed speed on 3D texture parameters for the two microscopically different materials.

For CTB010, a 75% decreased feed speed showed an increase of Ra by four times. At slower processing conditions (70 mms^{-1}), the target material has longer exposure time to absorb the laser irradiation: the matrix absorb the laser beam energy, convert it into thermal energy, metastable diamond is converted into stable graphite while Cobalt pool melt's expansion produces compressive stresses on diamond grains. For CTB010 this process caused a maximum profile valley depth (Rv) difference of 10.78 µm, as confirmed by white light interferometry. A change of ablation mechanism was noticed at different feed speed regions and a clear transition between the two distinguished machining mechanisms was identified (Figure 5a-c). This can be explained considering the effect of temperature on the binder. At 1768K the Cobalt pockets between the diamond grains melt and thus the local temperature of the melting pool increases. This means that there is the potential for the molten Cobalt to vaporise, which takes place at 3200K. Due to the transition from solid to gas, a volume expansion is created, causing a pressure on the melting pool which is known as the recoil pressure. For the metallic binder in the proposed experiment (Cobalt), the recoil pressure was calculated at 8.92 MPa based on previous research from Chen and Wang (2001) and Sun et al. (2017). Since Cobalt is 12% of the total mass, the effect of recoil pressure is not negligible. Furthermore, due to the higher thermal expansion coefficient of Cobalt compared to diamond (Table 1), prolonged compressive stresses in the diamond grains occurred due to the expansion of cobalt as previously demonstrated by Pacella et al. (2015). This caused the instantaneously converted amorphous carbon/graphite to be pushed at the side of the grooves simultaneously with ejected cobalt, later solidified (Figure 5a). This is also in accordance with previous research conducted by Pacella et al. (2014) where a combination of Transmission Electron Microscopy and Electron Energy Loss Spectroscopy allowed the identification of carbonic allotropes at increasing depths under the ablated surface. The extent of graphite was found to be proportional to the laser energy density and the Cobalt was found to undergo a repetitive process of ionisation with subsequent (partially overlapped) pulses due to its absorption coefficient, causing direct vaporisation of the superficial Cobalt in the infiltrated regions. This contributed to the formation of the elongated voids in the amorphous and graphite regions as the Cobalt progressively experienced its solid/liquid/vapour phase changes. EDX analyses revealed an increase of Cobalt in the range 14.8-29.8% weight when varying the speed from 210 mm s^{-1} to 350 mm s^{-1}, as shown in Figure 5b-c. Sun et al. (2017) demonstrated that when the feed speed is increased, the recoil pressure becomes lower, and, in this experiment, for speed in the range 200÷300 mm s^{-1}, a combined mechanism of machining due to both Cobalt pool melt ejection and dragging of amorphous carbon/graphite would dominate the process (Figure 5b). For feed speed above 300 mm s^{-1}, the milling mechanism could be explained by the phenomenon of Cobalt pool melt ejection (Figure 5c).

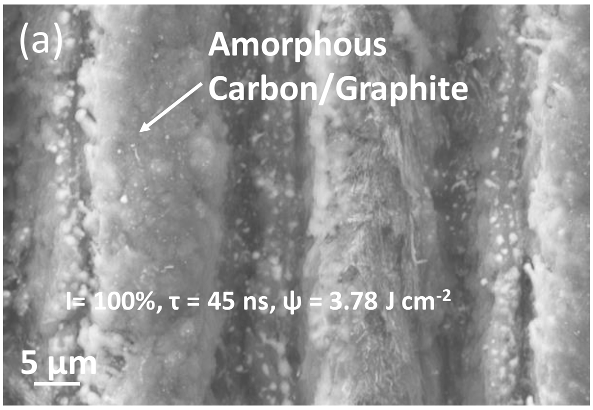

FS = 70 mm s^{-1}, τ = 220 ns, ψ = 11.34 J cm^{-2}

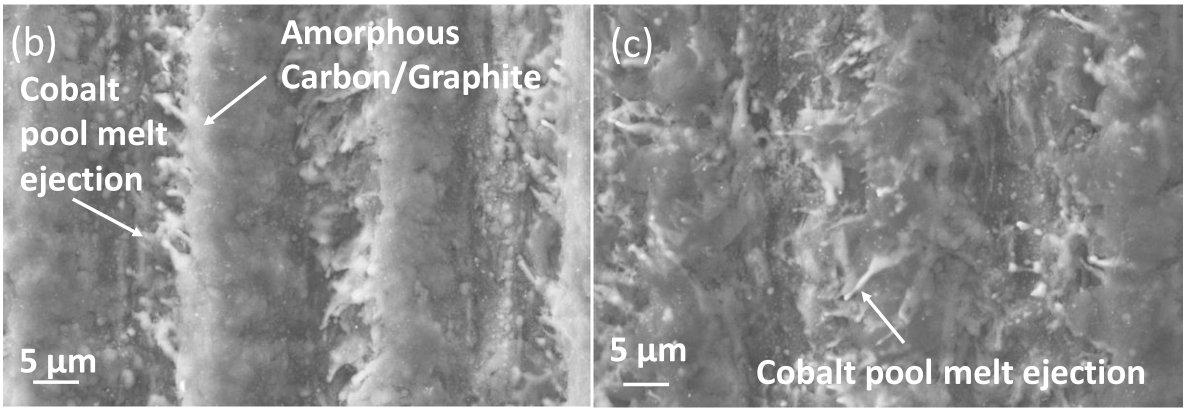

FS = 210 mm s^{-1}, τ = 220 ns, ψ = 11.34 J cm^{-2} **FS = 350 mm s^{-1}, τ = 220 ns, ψ = 11.34 J cm^{-2}**

Figure 5: SEM images of CTB010 laser milled surfaces at different feed speeds: a) 70 mm s^{-1} (Ra = 4.3µm), b) 210 mm s^{-1} (Ra = 1.6µm), c) 350 mm s^{-1} (Ra = 1.4µm).

At the same laser fluence (ψ = 11.34 J cm^{-2}) the two micro-structurally different PCD materials exhibit different milling mechanisms. For CTB010 a clear change in machining mechanism was found above laser feed speed in the range 200-350 mm s^{-1}; for CTM302 a clear transition from a process dominated by graphitisation/amorphisation of diamond into a process led by Cobalt explosion could not be identified. This can be explained considering the energy density irradiated on the target material during processing. In the nanosecond pulse regime, the energy threshold for a structure heavier in diamond (CTM302) is higher than for a structure lighter in diamond (CTB010), thus laser machinability is increased for higher content of Cobalt and smaller diamond grains. For a fluence value of 11.34 J cm^{-2} (laser intensity of 0.052 GW cm^{-2}), CTM302 did not reach the minimum threshold of energy density for milling coarse diamond grains, and this resulted in the Cobalt melting and being ejected. However, no conversion of diamond into graphite/amorphous carbon occurred. For laser feed speed below 200 mm s^{-1}, binder deposition appeared in the laser feed direction (Figure 6a), while above 200 mm s^{-1}, the mechanism of milling was dominated by Cobalt agglomeration at the grain boundaries (Figure 6b-c).

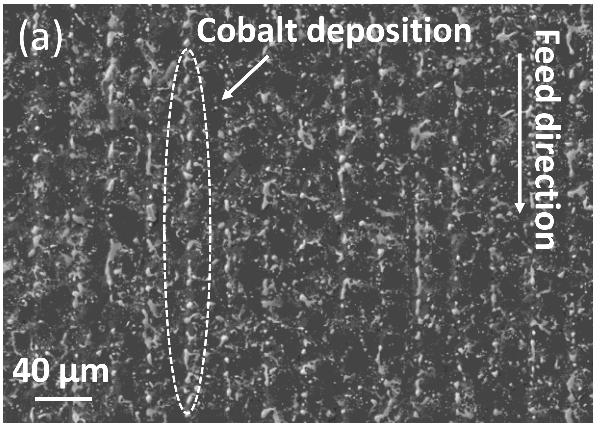

FS = 70 mm s^{-1}, τ = 220 ns, ψ = 11.34 J cm^{-2}

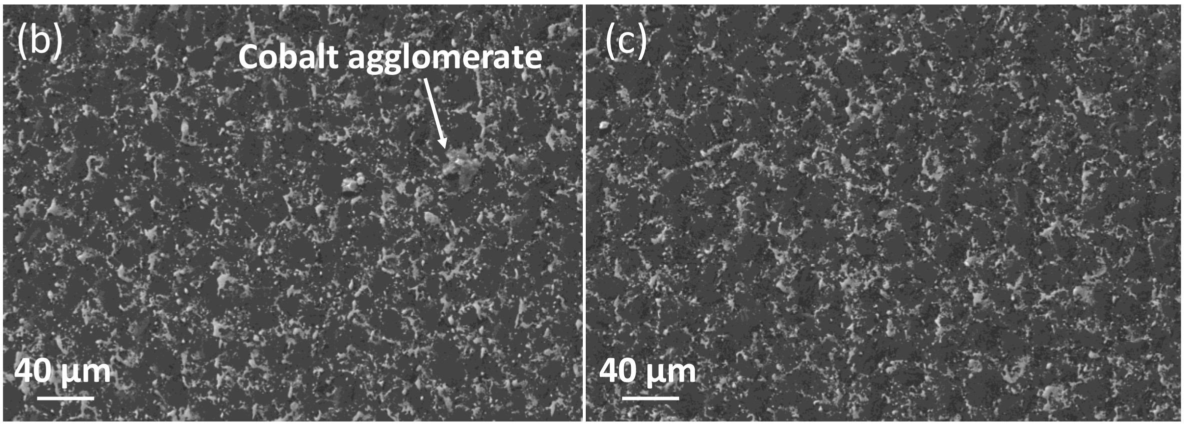

FS = 210 mm s^{-1}, τ = 220 ns, ψ = 11.34 J cm^{-2} **FS = 350 mm s^{-1}, τ = 220 ns, ψ = 11.34 J cm^{-2}**

Figure 6: SEM images of CTM302 laser milled surfaces at different feed speeds: a) 70 mm s^{-1} (Ra = 0.5µm), b) 210 mm s^{-1} (Ra = 0.41µm), c) 350 mm s^{-1} (Ra = 0.31µm).

3.2 Effect of track distance on the topography of milled textures

The second experimental study investigated the effect of track distance on the two-dimensional and texture parameters of the milled pockets.

A change in track distance induced distinct reactions in the two materials, possibly due to the different size of the crystallites. Figure 7a-d depict the effect of track distance on surface roughness Ra, Rk, Rpk and Rvk for both materials in the conditions of theoretical overlapping values of the beam area spots of 75% (for a feed speed of 350 mm s^{-1}), 85% (210 mm s^{-1}), and 95% (70 mm s^{-1}). A change in maximum, minimum and quartiles values of the presented boxplots is an indication of the effect of track distance on roughness parameters for the specific material. The dominating machining mechanisms are dependent on the microstructure and binder percentage; thus the mechanism of spot formation depends upon the diamond grain size. CTB010, which has diamond grains (10 µm) smaller than the programmed track distance (20-28 µm), is milled at higher removal rate in comparison to CTM302 and the effect of track distance is not negligible. This is seen in the interquartile range of the CTB010 boxplot (Figure 7) which are always above the ones for CTM302.

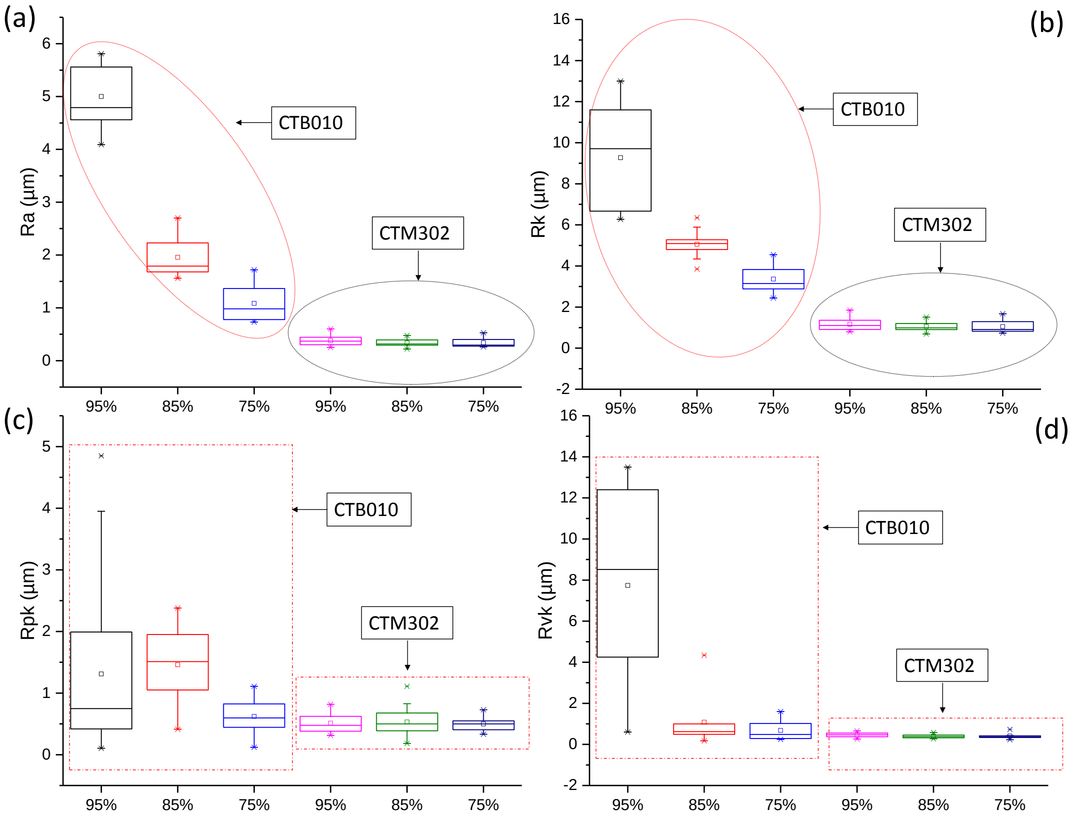

Figure 7: Effect of track distance at different spot overlaps and its influence on surface roughness parameters in CTB010 and CTM302.

For CTM302, a variation in track distance did not affect the ablation mechanism, this is represented in Figure 7 by the flat plateau in Ra, Rk, Rpk and Rvk for all CTM302 fitted data and in Sk, Spk and Svk in Figure 8. A high dependence of Ra and Rk from spot overlap for CBT010 (Figure 7a, b) and a similar trend for their 3D counterparts (Figures 8a, c) were found. For CTB010 only 95% spot overlap resulted in an increased Rvk: average depth of the profile valleys projecting through the core profile (Figure 7d).

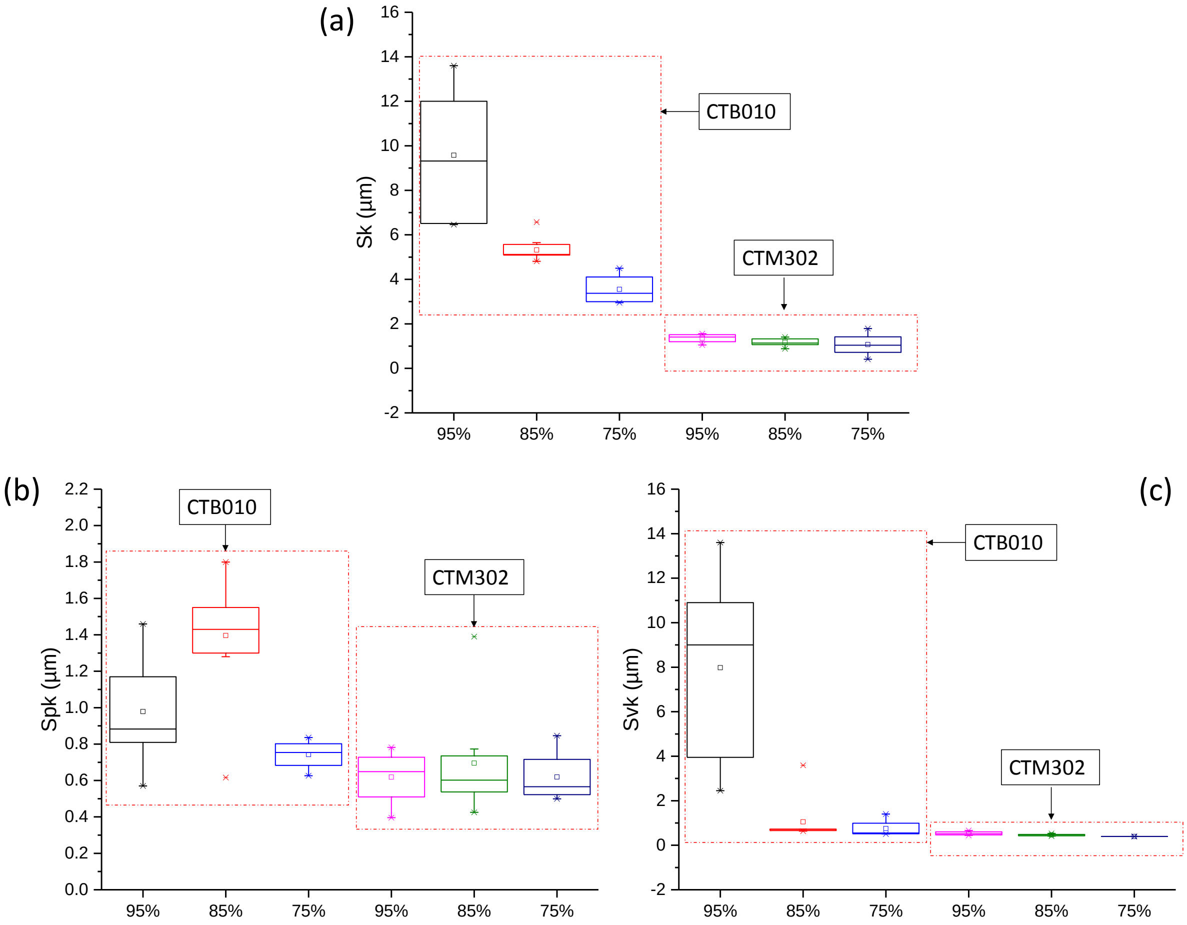

Figure 8 Plot of spot overlap variation and its effect on surface roughness parameters in CTB010 and CTM302.

The main consideration that can be drawn upon discussed results is that when processing polycrystalline structures, a track distance smaller than the hard grain size should be used to minimize the effect of track distance on surface roughness and to maximise the dependency of surface roughness on feed speed. The effect of pulse overlap is also evident in Figure 7: the higher the pulse overlap, the higher the roughness. In general, when a larger pulse overlap is used, the exposure time of the target material to the laser beam is longer. In milling CTB010 the relation between pulse overlap and surface roughness is based on an exponential relation, which becomes nearly linear for CTM302. This is due to the higher binder content in the CTB010. For both materials, the pulse duration (ns) is longer than the Cobalt's relaxation time (fs); thus, vaporisation occurred in the laser pulse timeframe. This is in accordance with previous research from Hoffman (2015). Pacella et al. (2014) demonstrated that the high absorption and lower vaporisation enthalpy of Cobalt (382.4 $Wm^{-1}K^{-1}$) is responsible for enhancing the process of increased temperature/vaporisation/ absorption during laser processing. Considering the materials selected for the experiments, this explains why materials with higher Cobalt content (such as CTB010) result in higher roughness post laser processing.

3.3 Effect of numbers of passes and depth of cut on the strengthening mechanism

The effect of programmable parameters such as depth of cut (layer thickness) and number of passes (number of layers) was studied and the effect of diamond grain size and Cobalt binder extent were investigated. It was found that depth of cut and number of passes noticeably affect the laser/material interaction and, subsequently, the material's surface integrity/properties such as surface roughness and micro-hardness. When machining CTM302 with smaller depths of cut and multiple passes (Figure 9b), a decrease of surface hardness (48.4 GPa) was noticed, while machining at higher depth of cut (Figure 9c) led to an increased hardness (203.7 GPa). These values were compared to the benchmark hardness of the as-received CTM302 sample which was measured at 72.2 GPa (Figure 9a). For polycrystalline materials, which grain size and distribution are variable, the observed phenomenon suggests that the multi-layer milling process is not purely based on the thermal properties of materials, but an important role is played by the mechanical forces generated by the possible action of a recoil pressure, which is also confirmed by Ochsner and Holm (2016). When multiple layers of materials are machined, the effect of recoil pressure is more pronounced. Deng and Molian (2012) also demonstrated that the wave produced by the recoil pressure can propagate in the underneath structure beyond the molten layer producing compressive stresses in the substrate. Furthermore, during multi-layer processing, a possible accumulation of compressive stresses on the diamond grains might dominate the process for CTM302, as also reported in previous research by Miess and Rai (1996).

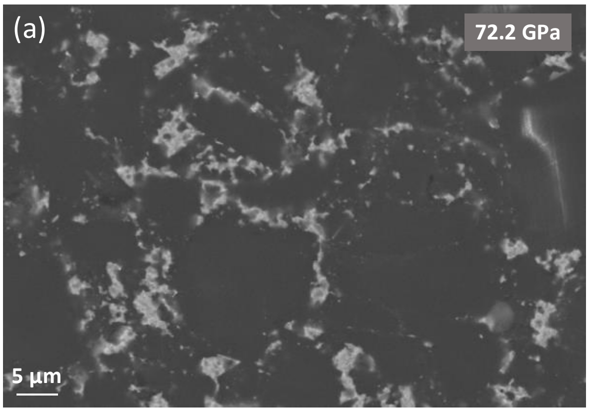

As-received

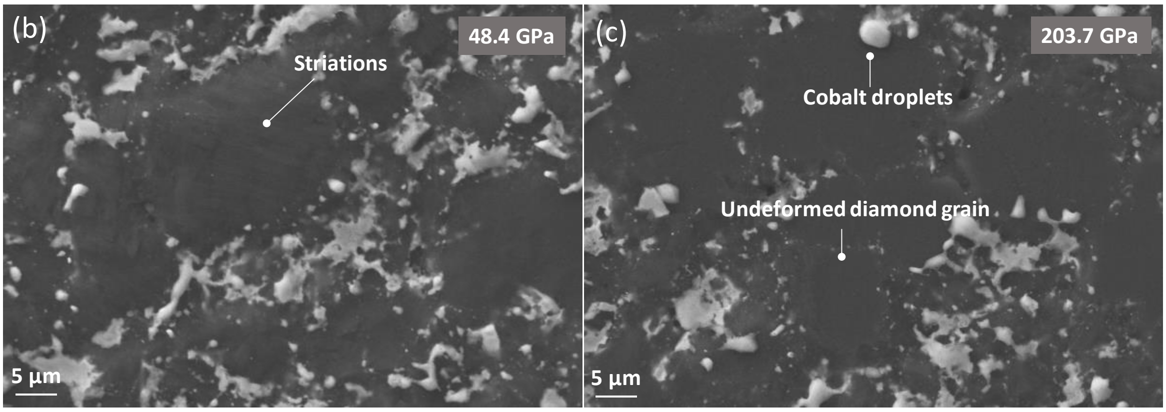

FS = 1000 mm s^{-1}, ψ = 11.34 J cm^{-2}, N = 5, doc = 1 µm **FS = 1000 mm s^{-1}, ψ = 11.34 J cm^{-2}, N = 1, doc = 5 µm**

Figure 9: SEM images of CTM302: a) as-received sample, b) milled at 0.57 mJ in condition C5, c) milled at 0.57 mJ in condition C4. Details of the conditions can be found in Table 4.

At shorter pulse durations and smaller fluences an increase of number of milled layers (Figure 10b) caused a reduction of hardness (95 GPa), which is still above the as-received structure (72.2 GPa) but lower than the one achieved in processing condition D5 (258.4 GPa) as shown in Figure 10a. Processing condition C2 (Figure 10b) enabled achieving a microstructure where striations were present within the grains and the grains were reduced in size compared to the original microstructure. The striations (Figure 10c) could indicate that a solidification process occurred within the crystallites. The combination of heat treatment at low fluence (3.78 J cm^{-2}) and a change in rate of solidification between each pass due to the accumulation of local heat, may have contributed to a change of grain size now in the order of 10 µm as opposed to the as-received crystallites (approximately 30 µm). The result agrees with the Hall-Petch strengthening effect (Hall, (1951); Petch, (1953)) for which by changing the average crystallite size it is possible to strengthen polycrystalline materials. Furthermore, a change in grain size also affects dislocation movement, hence, by reducing the crystallite size more grain boundaries are formed which impede dislocation movements and affect yield strength.

The effect on the obtained structures also resemble the typical laser shock peened surfaces, as explained in research from Dahotre and Harimkar (2008) and Shukla et al. (2015). These processing conditions might have favoured a hybrid process in which both the initiation of an ablative mechanism and laser shock processing could coexist. Consequently, a combination of compressive stresses due to both the mismatch of thermal expansion coefficient (between Cobalt binder and diamond grains) and a shock wave could have caused a microstructural change and an increase in hardness (from 72 to 95 GPa).

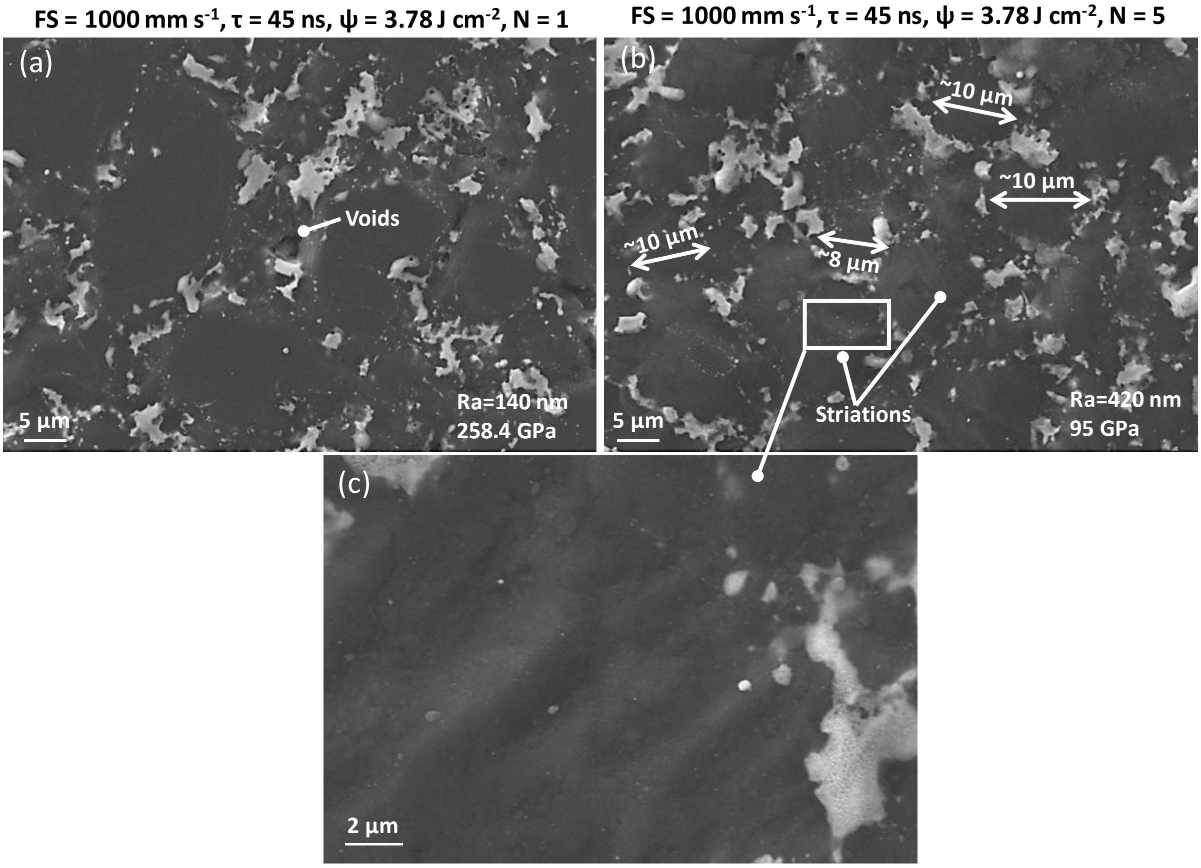

Figure 10: Effect of increased number of passes for CTM302 (TD = 20µm, doc = 1µm): a) 1 pass (condition D5), b) 5 passes (condition C2), c) magnified detail of striations in one of the crystallites.

The observed reaction in the milled pockets of CTB010 and CTM302 at the same energetic conditions (Figure 11) suggests that the main differentiating factor in the two polycrystalline structures is the presence of mechanical forces of different extent. CTB010 and CTM302 differ in grain size and grain distribution, the local positioning of the diamond grains increases the local strength, thus CTM302 materials exercise higher local strength. When the laser beam hits the target, the beam energy is converted to thermal energy, resulting in the ablation of the first layer. The successive layers in CTM302 possess higher binding energy, thus are more difficult to be milled, however, phenomena of diffusion and absorption occur which cause the binding energy to decease making the ablation possible. The binder content variation between the two machined structures affects the extent of molten material which will be higher for CTB010. This introduces loss of bonding between diamond grains. This also justifies why an exponential relationship between numbers of passes and surface roughness was found for CTM302 while this was linear for CTB010. In CTB010, since the grain size is circa 10 µm, the increase in number of passes is proportional to the number of grains involved during processing which makes this PCD grade an easier option for repeatability and easy to control processing. CTM302 is unpredictable due to its multi-modal structure and a dimensional gap of 25-28 µm between grains.

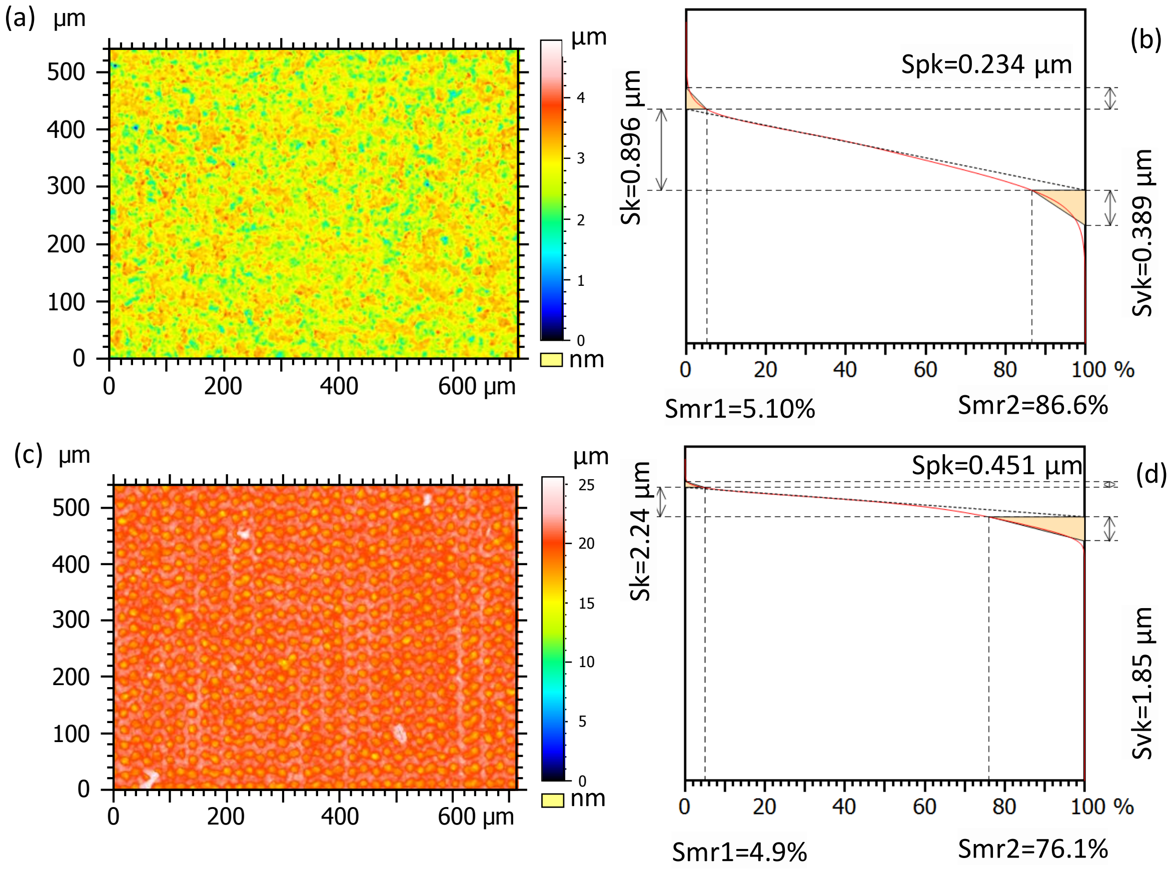

Figure 11: Alicona 3D images and Abbott curve for one surface of CTM302 (a, b) and CTB010 (c, d) milled surfaces at τ = 220 ns, ψ = 11.34 J cm^{-2}, I= 100%, FS = 1000 mm s^{-1}, TD = 20 µm, N=1, doc = 1 µm.

3.4 Effect of irradiated energy on the milling mechanism

Dahotre and Harimkar (2008) and later Hoffman (2015) demonstrated that laser machining of brittle materials is a complex process, in which explosive boiling, ejection melt, and the generation of a recoil pressure may coexist. Figure 12 is a schematic of the two milled materials at a fixed fluence of 11.34 J cm^{-2} at variable feed speeds. Distinct milling mechanisms were identified for the two materials. For CTB010, since 11.34 J cm^{-2} is above the material's ablation threshold the dominant milling mechanism is purely thermal: a larger area of liquid flow is formed due to the higher Cobalt binder (12% in weight), thus the process of melting and ablation of Cobalt weakens diamond's granular bonding forces, resulting in a higher material removal rate and higher surface roughness, as previously shown in Figure 5. A cavity is left from the transition of solid diamond to vaporised carbon, porous graphite might form at the vaporised interface and graphitisation might occur due to the transition of metastable diamond to stable graphite. For CTM302, a fluence of 11.34 J cm^{-2} is below the material's ablation threshold, thus the resulting mechanism is purely thermal on Cobalt, and purely mechanical on the crystallites: higher grain-to-grain bonding forces prevent milling.

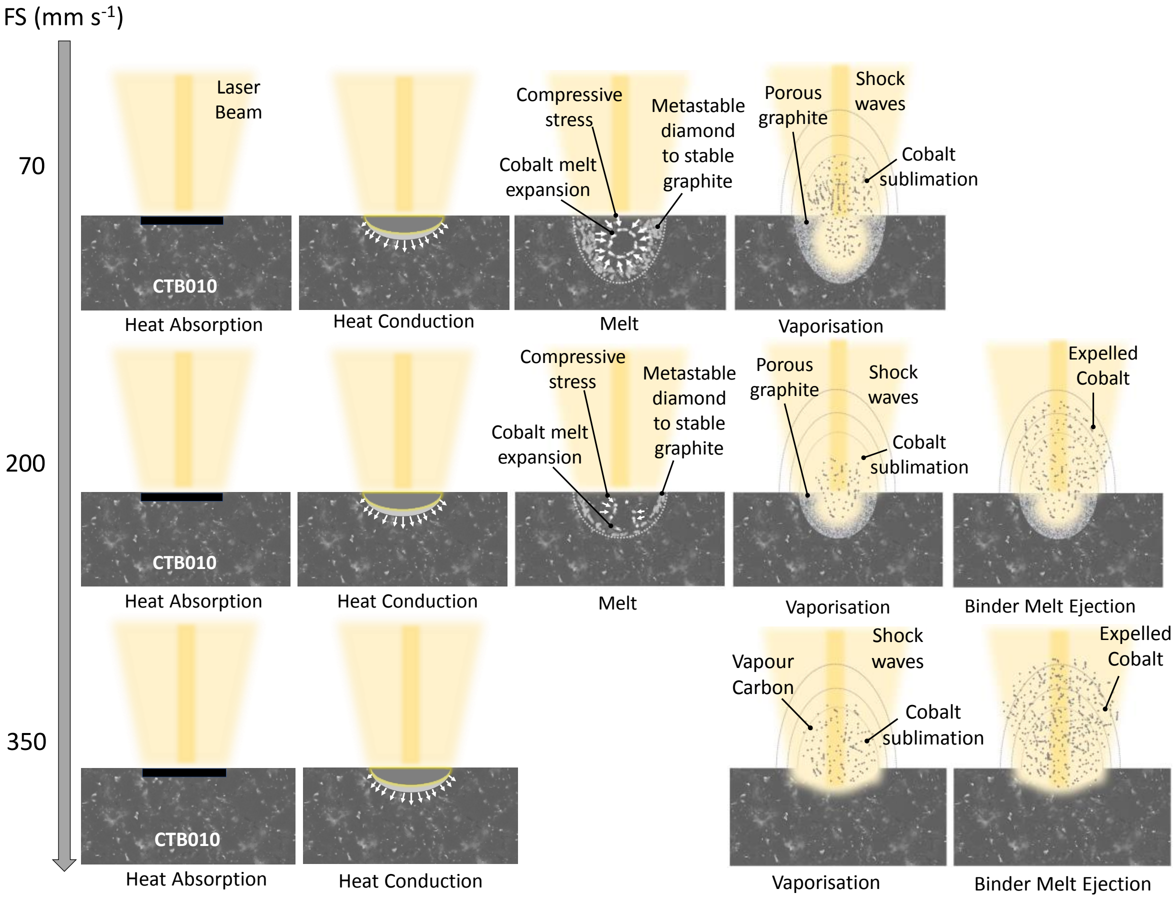
FS (mm s⁻¹)
70
200
350
Laser Beam
CTB010
Heat Absorption
Heat Conduction
Compressive stress
Metastable diamond to stable graphite
Cobalt melt expansion
Melt
Porous graphite
Shock waves
Cobalt sublimation
Vaporisation
Expelled Cobalt
Binder Melt Ejection
Vapour Carbon

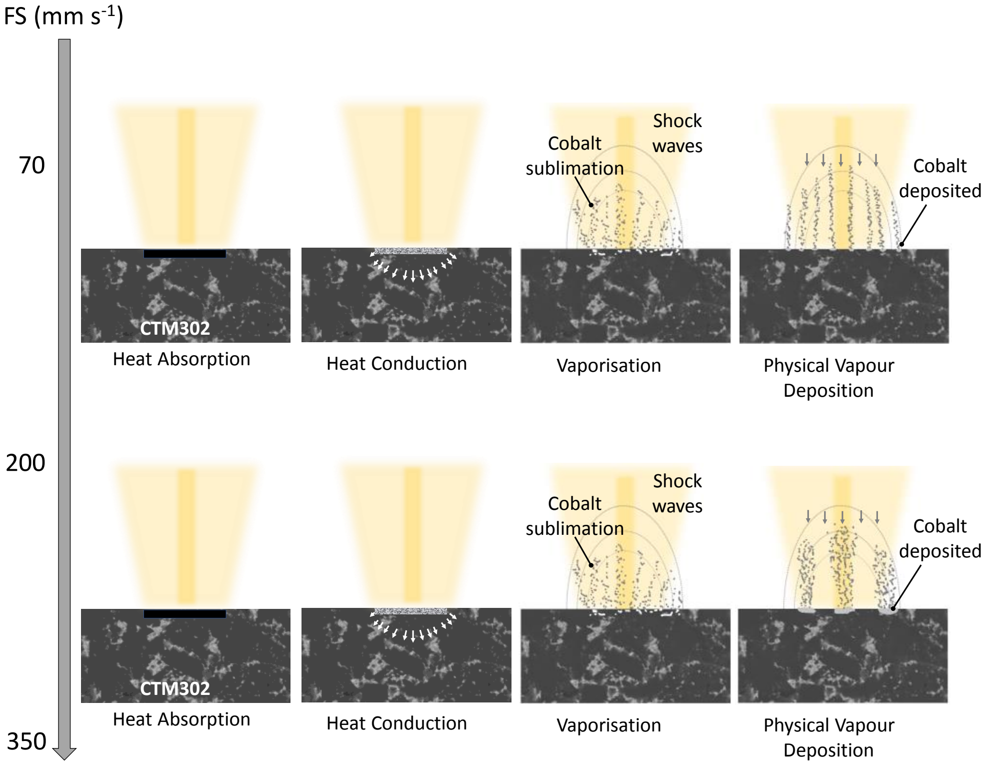
FS (mm s⁻¹)
70
200
350
CTM302
Heat Absorption
Heat Conduction
Cobalt sublimation
Shock waves
Vaporisation
Cobalt deposited
Physical Vapour Deposition

Figure 12: A schematic of the milling mechanism for the two microstructurally different materials at the same conditions: I = 100%, τ = 220 ns, ψ = 11.34 J cm^{-2}, TD = 20 µm, N=1, doc = 5 µm.

Milling of pockets using different waveforms (i.e. different pulse duration and energy density) resulted in a variation of spot density per surface area, aspect ratio, surface roughness and micro-hardness. For CTB010, when shorter pulses (45 ns compared to 220 ns) are irradiated at higher frequency (105 kHz compared to 35 kHz), the fluence is reduced to 3.78 J cm^{-2} (compared to 11.34 Jcm^{-2}) however the irradiance is increased to 0.084 GW J cm^{-2} (compared to 0.052 GW J cm^{-2}) calculated based on previous research by Pacella et al. (2014). The increase of irradiance revealed a lower surface roughness Ra (0.88 µm compared to 1.37 µm), and more homogeneous spot distributions. A reduction of laser fluence at a track distance of 28 µm resulted in a reduction of core roughness Sk, and an increase of Spk (Figure 14 a-b). However, milling at a track distance of 20 µm improved Ra (Figure 13c-d), and reduced the effect of energy density on the Spk values, which are now similar at lower (3.78 J cm^{-2}) and higher (11.34 J cm^{-2}) fluencies (Figure 14) and only 100nm above the Spk of the as-received sample (Figure 2). These Spk values prove that ablation of CTB010 at low and high fluences does not significantly affect the material's wear properties.

A combination of laser beam paths strategies as well as energetic considerations are therefore required in processing polycrystalline materials with grain size between 2 and 10 µm.

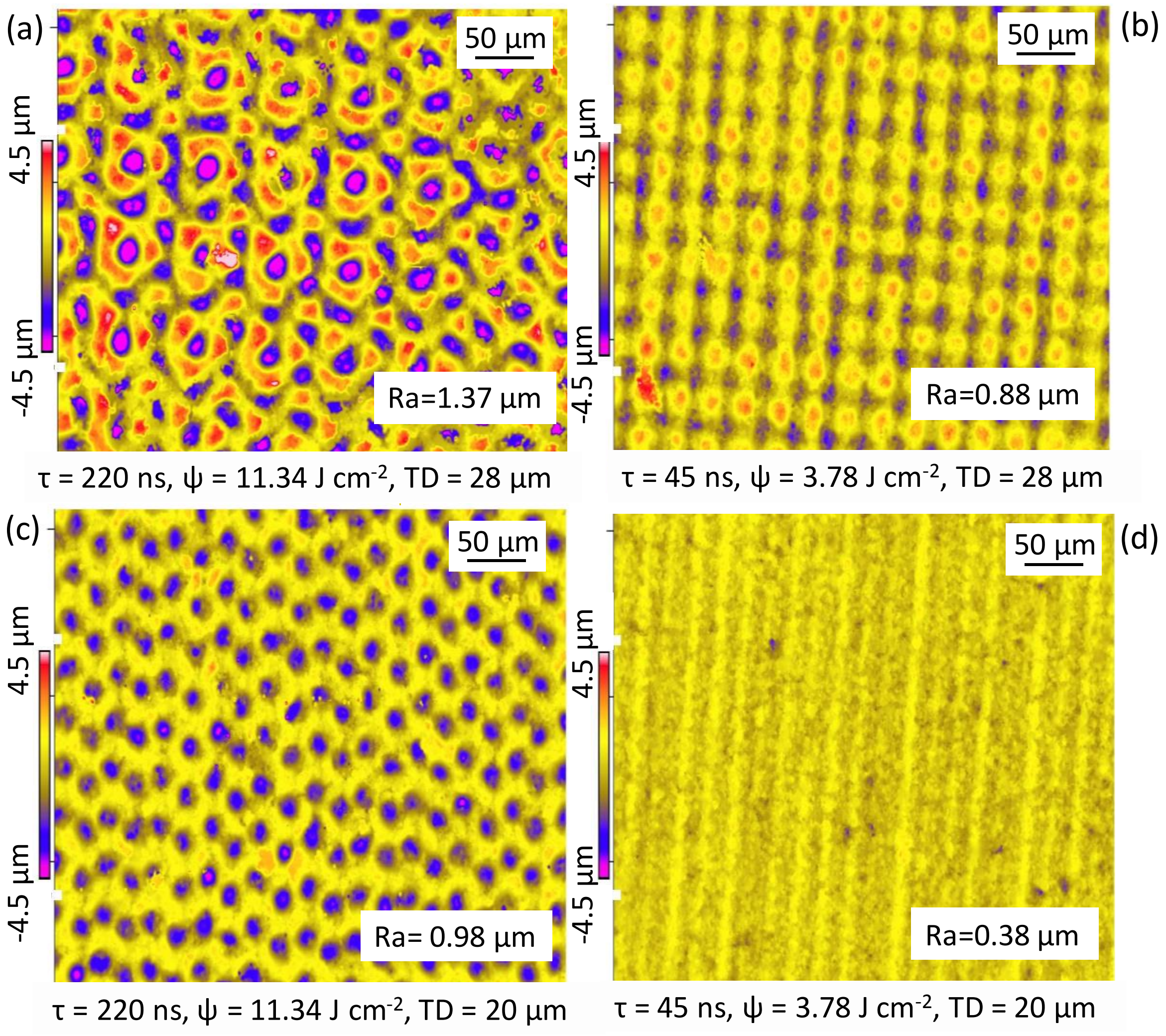

τ = 220 ns, ψ = 11.34 J cm^{-2}, TD = 28 µm

τ = 45 ns, ψ = 3.78 J cm^{-2}, TD = 28 µm

τ = 220 ns, ψ = 11.34 J cm^{-2}, TD = 20 µm

τ = 45 ns, ψ = 3.78 J cm^{-2}, TD = 20 µm

Figure 13: Topographical profile of CTB010 milled surfaces at I= 100%, FS = 1000 mm s^{-1}.

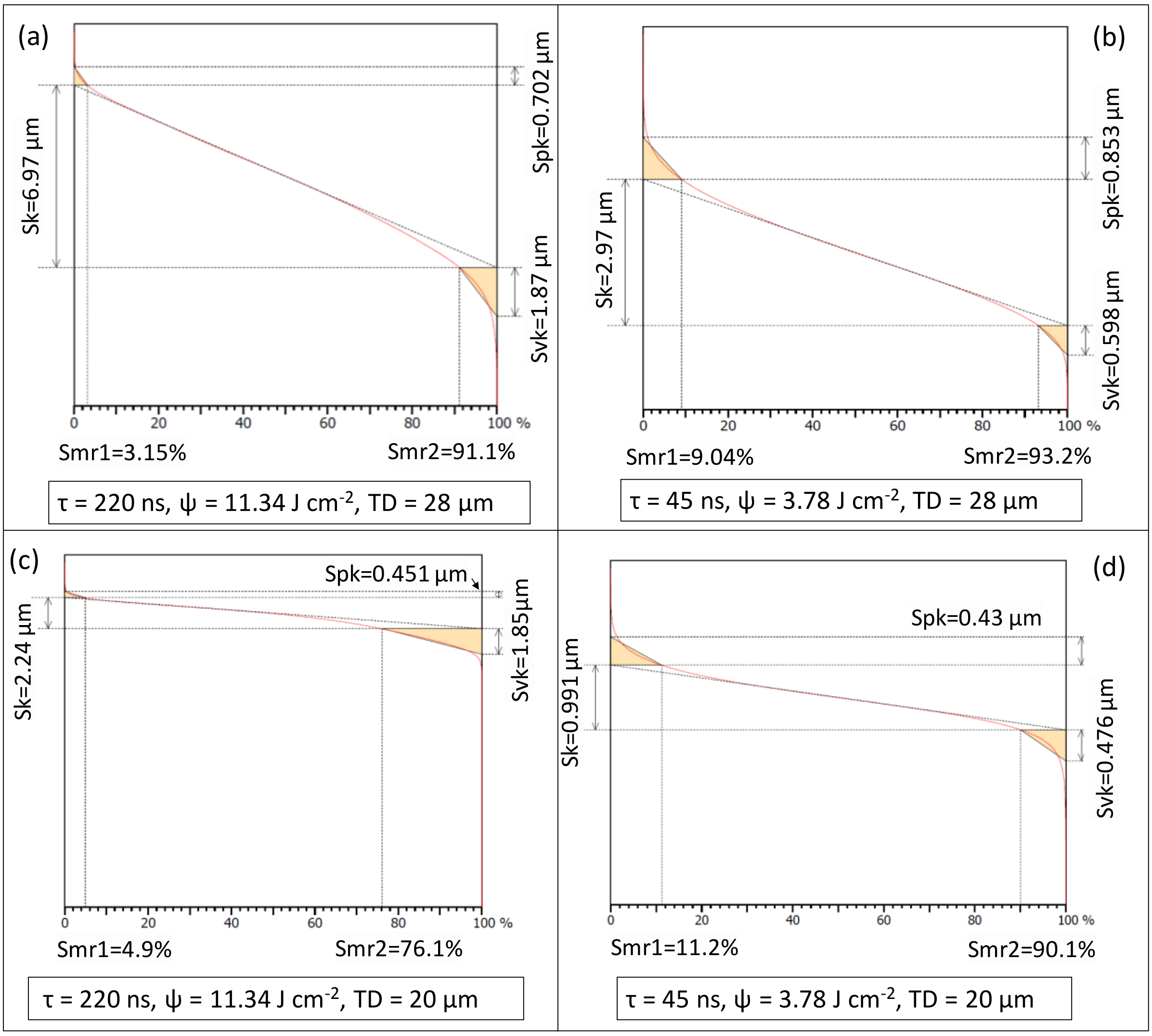

Figure 14: Abbott curve for one surface and parameters Sk, Spk, Svk of CTB010 milled surfaces at I= 100% and FS = 1000 mm s^{-1}.

For the multimodal grade CTM302, a change of waveform (i.e. frequency and fluence) and pulse duration resulted in similar values of 3D roughness values Spk with a maximum difference of 30% compared to CTB010 (Figure 15). This is due to the grain size of the CTM302 structure. The combination of coarse and fine grains makes CTM302 structure more thermally stable, thus providing a higher energy milling threshold. The reduced binder fraction (2% reduction) and increased diamond grain size provide an increase in binding forces between grains due to the extended intergrowth area. Previous research by Pacella et al. (2014) which employed an Nd: Yag pulsed laser (100 W) with a microsecond pulse duration showed no difference in the milling rate and mechanism between the two composites at fluences between 623-7369 J cm^{-2}. This range of fluence is well above the energy threshold for both grades. Research from Deng and Molian (2012) stated that in high-energy-density regime, the mechanism of material removal trough laser machining for composites is a combination of thermal and photophysical processes. The proposed findings indicate that for polycrystalline materials at lower laser fluences (1-20 J cm^{-2}), a small difference in metallic binder fraction (% 2 in this case) may cause a major variation in the minimum energy-ablation threshold and laser-processing rates. This is in accordance with the two-temperature model for metals proposed by Christensen et al. (2007): at lower laser fluence, energy is transferred only within the absorption depth, whereas at higher laser fluence the energy distribution occurs through thermal diffusion length. This new finding also introduces mechanical forces as crucial factor in laser beam-polycrystalline diamond interaction at lower fluences.

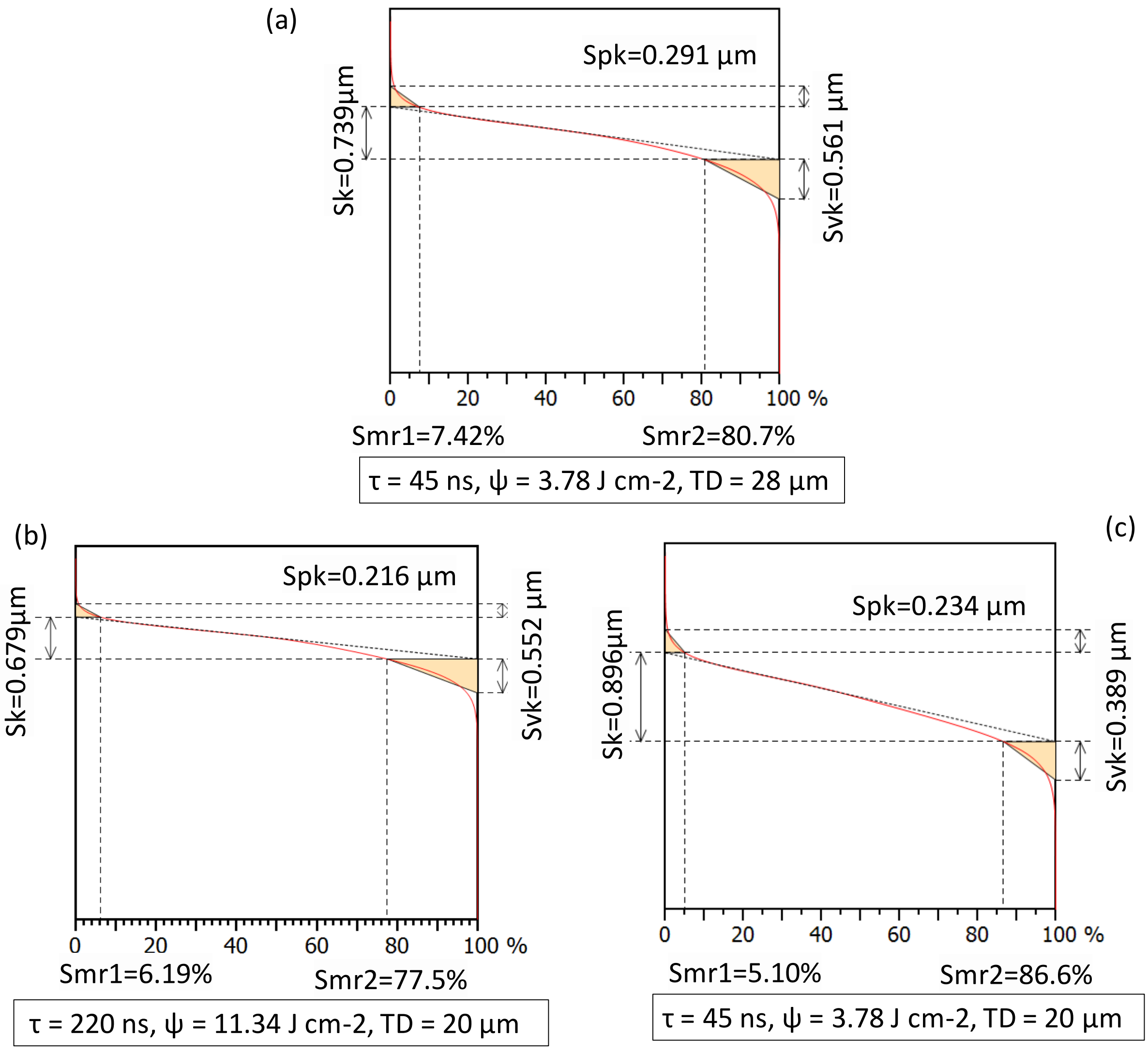

Figure 15: Abbott curve for a single profile and the parameters Sk, Spk and Svk of CTM302 milled at I 100%, FS 1000 mms^{-1}.

Micro-hardness measurements of the processed areas showed that the irradiated energy is a primary criterion for microstructure surface engineering since this strongly affects the final hardness of the composites. At high feed rate (1000 mm s^{-1}) for fluence of 11.34 J cm^{-2}, a micro hardness of 48.37 GPa was achieved (condition C5); while reducing the fluence to 3.78 J cm^{-2} (condition C2) resulted in hardness of 95.7 GPa.

EDX analyses on the milled pockets at conditions C2 ($I = 100\%$, $\tau = 45$ ns, $\psi = 3.78$ J cm^{-2}) and C3 ($I = 100\%$, $\tau = 220$ ns, $\psi = 11.34$ J cm^{-2}) revealed a change in microstructure and an increase of the superficial binder's fraction without any induced surface damage (Figure 16). Previous investigation from Pacella et al. (2014) showed that for fluences above 623 J cm^{-2} an increase of Cobalt occurred in the ablation of both CTB010 and CTM302, however this was accompanied by high material removal rate, a reduction of surface integrity and graphitisation. In this paper, adopting a lower range of fluence (<20 J cm^{-2}) on multi-modal composite CTM302 led to an increase of Cobalt at the ultra-hard intergranular boundaries (Figure 16b) and good surface integrity (Ra = 140 nm). In the region milled at low fluence the increase of Cobalt could be caused by the surface pressure achieved. Previous study by Yudasaka et al. (1998) demonstrated that for low ablation pressures, the energy would be absorbed by the diamond's grains and converted into thermal energy, while Cobalt would reflect the laser beam which may limit its temperature increase. It was also demonstrated that there is a direct proportionality between laser intensity and recoil pressure. In the conducted experiment, since the laser intensity is below 0.084 GW cm^{-2}, the recoil pressure can be estimated at circa 8.92 MPa using the model proposed and validated by Chen and Wang (2001). Thus, at temperature of 4000 K diamond grains would absorb the energy and evaporate, reducing the transfer of thermal energy to Cobalt and therefore impeding the increase of temperature necessary to allow its vaporisation. As a result, more Cobalt would remain on the milled surface (Figure 16).

An increase of energy per pulse (fluence = 11.34 J cm^{-2}) revealed a microstructural surface modification which led to an increased binder volume and a reduction of average grain size (Figure 16b). The achieved microstructure is ideal for complex tools where roughing operations are needed before the final finishing process and there could be a potential applicability of the surface engineered structure to be employed for profile routers and thread cutting tools or wear part applications.

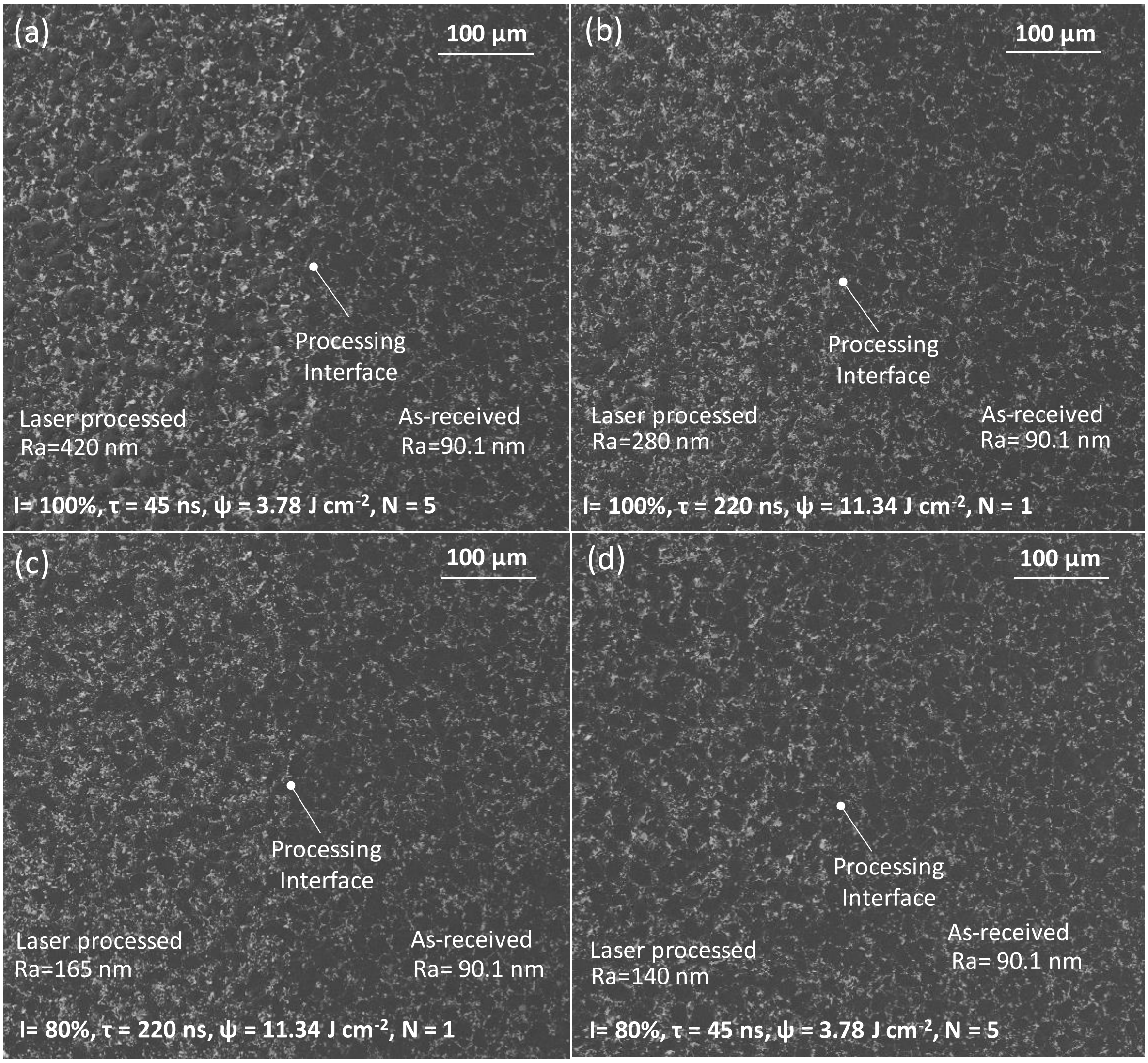

Figure 16: SEM micrographs of CTM302 milled surfaces.

In milling CTM302, an increase in the extent of Cobalt, as measured through EDX analyses, and a minimum surface roughness of 140 nm at 0.19 mJ per pulse (Figure 16d) were achieved. Topographical measurements revealed that a reduced intensity is required in laser milling especially when improved roughness is needed. A 20% decreased power showed 50-70% improvement in roughness. In the case of CTM302, conditions C4 (I = 80%, τ = 45 ns, ψ

= 3.78 Jcm^{-2}) and D4 (I = 80%, τ = 220 ns, ψ = 11. J cm^{-2}) caused a surface roughness Ra of 165 and 140 nm, respectively, these values are slightly rougher than the as-received surface (90.1 nm). Deng and Molian (2012) claimed that, due to laser shock processing of PCD materials, inhomogeneous microstructures and rougher surfaces would be achieved; however, results presented in this paper show that a homogeneous microstructure and binder distribution can be achieved through a low-energy laser thermal process (Figure 16c-d).

For laser fluences below 10 J cm^{-2}, although plasma plume absorbs part of the energy, some energy is radiated back onto the target, enhancing target's surface temperature, while the remaining is radiated into the opposite direction, this result is in accordance with research conducted by Vasantgadkar et al. (2010). The CTM302 milled surface at low fluence exhibited Cobalt etching because insufficient energy was absorbed by the PCD structure to ablate diamond grains from the target material. The effect of binder fraction on the surface roughness at different laser irradiance values is shown in Figure 17. CTM302 exhibits better surface roughness and faster processing rates than CTB010.

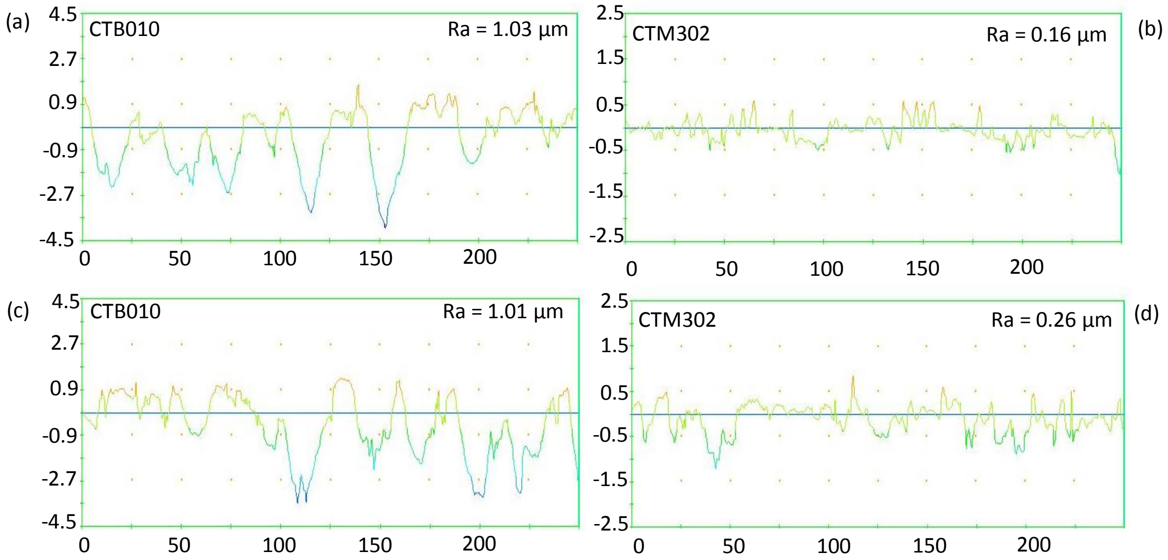

Figure 17: Surface roughness profiles of CTB010 and CTM302 (FS 1000 mms^{-1}, ψ = 11.34 J cm^{-2}, τ = 220 ns, TD = 28 µm) at: I = 80% (a, b); I = 100% (c, d).

This is an interesting result caused by an increase of metallic binder volume present in the CTB010 as well as different thermal properties of the ultra-hard grains and Cobalt (Table 1). The laser milling process proposed in this paper provides an alternative solution to conventionally industrially utilised processes of electro discharge grinding, particularly for finishing applications. Ra, Rk, Rpk values derived from the Abbot-Firestone's curves for CTB010 and CTM302 are reported in Figure 18. The selected processing conditions on the X axis of each graph correspond to the milling parameters for which improved micro-hardness was recorded.

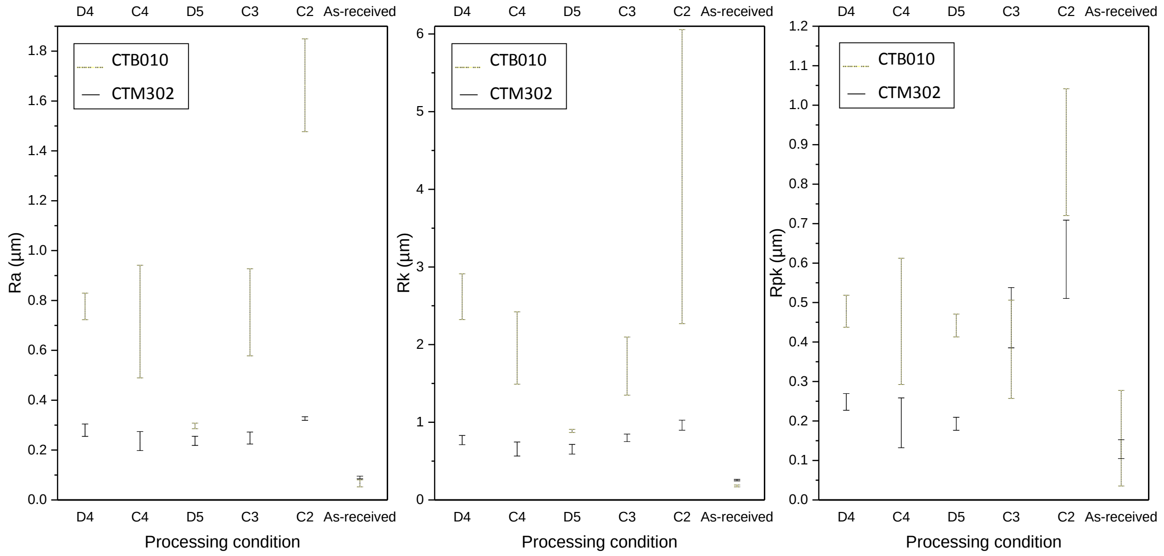

Figure 18: Measurements of 2D roughness parameters extracted from Abbott-Firestone's curves at different processing conditions.

A research conducted on CTB010 and CTH025 by Thoe et al. (1996) evaluated the effect of microstructure change in roughing and finishing application through EDG. They concluded that the grind-ability of finer grain size polycrystalline diamond was better than coarse diamond grains, and that the minimum edge finish achievable was 1.4 µm for CTB010 and 2.8 µm for CTH025 (average grain size 25 µm, Cobalt binder volume, circa 10%). This study revealed a different trend for thermal processing of polycrystalline diamond composites in which the utilisation of a laser irradiance below the energy threshold can promote good surface integrity an improved surface roughness values in comparison to EDG: a minimum roughness Ra of 0.54 µm was achieved for CTB010 and 0.14 µm for the multi-modal CTM302. The thermal processing is highly affected by the metallic binder content where the lower the volume of metallic binder is, the better surface roughness can be achieved. CTM302 is more sensitive to a variation of laser power, as shown by an increased surface roughness from 0.16 µm to 0.26 µm in Figures 17 b-d.

3.5 Effect of laser parameters on micro-hardness

The results of the hardness measurements revealed an increased micro-hardness for an increase in laser feed speed. Figure 19 shows the hardness measurements at a constant load of 500 mN for the as-received sample as well as all the processed samples for CTM302. The hardness of the as-received sample was measured at 72.2 GPa (indicated as CTM in Figure 19). Laser machined surfaces at low feed speed processing condition C1 (70 mms^{-1}) and D6 (350 mms^{-1}) showed material softening up to 40.6 GPa and 61.8 GPa respectively (Figure 19). This is possibly due to the thermal-induced dynamic recovery in the material caused by an increased temperature. The low feed speeds used in these processing conditions might have favoured an accumulation of heat and an increase of local temperature. Condition C4 increased the hardness to 203.7 GPa.

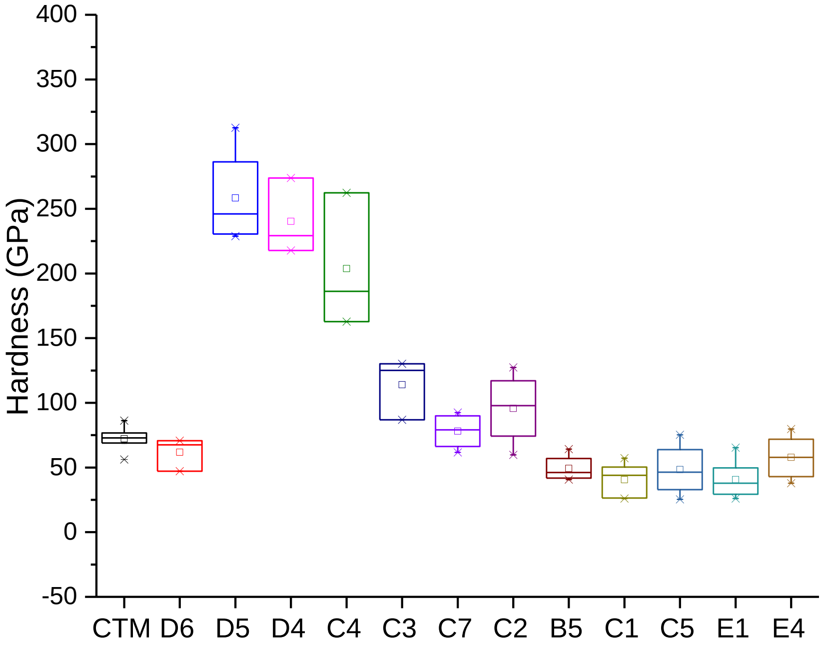

Figure 19: Graph of average measured valued of micro-hardness at a load of 500 mN in different processing conditions for CTM302 (CTM represents the the as-received sample).

Since the load was kept constant at 500 mN, the hardness at the correlated depth for each material is reported in Figure 20. This is an indication of the extent of elastic/plastic deformation induced by the constant load which shows that for longer pulse length and higher fluences (conditions C3), a micro-hardness of 114.02 GPa was achieved at a depth of 870 nm. However, it should be noticed that decreasing both laser intensity (by 20%) and track distance (condition C4) led to an increased hardness of up to 203.7 GPa at 450nm (70% higher than the as-received sample) and a roughness Ra of 160 nm, compared to 280 nm in condition C3 (Figure 20). For shorter pulses and lower fluences (conditions C2 and

D4), the effect of decreasing intensity (by 20%) was more pronounced and led to an increased hardness (95.69 GPa, at a depth of 750 nm versus 240.29 GPa, at a depth of 670nm) and an improved roughness (420 nm for C2 and 140 nm for D4). Among all, condition D5 resulted in the highest hardness (240.36 GPa) at the lowest laser irradiance and the material retained this hardness at a depth of 350 nm. In all the cases track-distance did not have a major effect on achieved hardness and roughness, however, when machining at a deeper depth of cut, an improvement in hardness was revealed. A possible cause for an increased hardness up to 203.7 GPa achieved at a depth of cut of 5 µm might be found in the strengthening effect due to the combination of heat treatment and plastic deformation of the crystallites. The enhancement of hardness due to heat treatment or a change in rate of solidification was firstly demonstrated by Hall and Petch (Hall, (1951); Petch, (1953)). A deep cut (5µm) in condition D4 might have induced favourable conditions for an accumulation of heat in the cutting zone, causing plastic deformation as suggested in Figure 21b. Furthermore, due to the repeated number of passes (N=5), the process of heat treatment post plastic deformation might have occurred multiple times, promoting an increase of hardness.

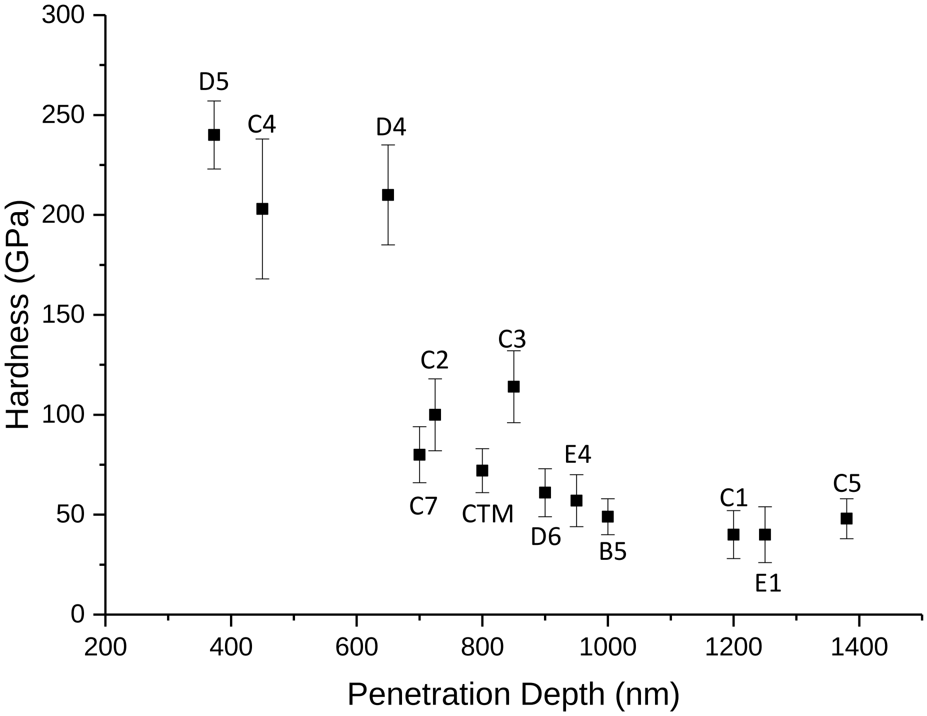

Figure 20: Graph of micro-hardness measurements as a function of the indentation depth at 500mN.

Haag et al. (2014) defined the Indentation Size Effect (ISE) as the apparent variation in the perceived material properties (hardness and elastic modulus) with the load of indentation. Figure 21a show the load dependence of the measured micro-hardness of the processed and as-received samples. The measured hardness decreased noticeably with increased applied load, particularly below 1500 mN. Previous research on nanotwinned diamond also showed a reduction of Vickers hardness at increased applied load: hardness reduced up to 80% when the load was increased by 4 N (Tao et al. (2017)) while the reduction reported by Huang et al. (2014) was up to 100% when the load was increased by 2 N.

The rapid decrease in hardness with increased load is mainly due to loss of elastic recovery in the materials and plastic deformation start occurring. This phenomenon can be described based on research conducted by Haag et al. (2014), which showed that due to dislocation activations, strain softening can occur in plastic deformation rather than strain hardening. In shallow indentations, the plastic zone is quite small to have enough dislocations and, hence, dislocations operate at limited locations resulting in an increase in hardness. For large penetration depths, a continuous process of accumulation of more dislocations during deformation can induce strain softening, and this softening is the source of ISE. In addition, the variation of hardness can be induced by damage evolution. This is in accordance with the pioneering work of Leimatre and Dufailly (1985) whose indentation approach was used to quantify deformation-induced damage through the degradation of indentation hardness and modulus. The average flow response of the materials under the indenter can be measured through the mean effects of all voids and discontinuities on the mechanical properties, which result in the direct damage measurements. This was later validated by Tasan et al. (2009).

The measured hardness for D4 and C2 reduced sharply with increased load, denoting an increasing damage, up to 70% and 40% respectively at 2500mN load (Figure 21a). The main processing differentiating factor for D4 and C2 was the depth of cut of the milled layers, which were respectively 5 µm and 1 µm. When multiple layers of materials were machined, the effect of recoil pressure was more pronounced. The wave produced by the recoil pressure could propagate in the underneath structure beyond the molten layer producing compressive stresses in the substrate, thus the superficial hardness was found to be initially higher for higher depth of cut, and then similar for the two conditions (D4 and C2) at 2500 mN. The results suggest that a major amount of damage was accumulated in the material, which led to a sudden decrease in its hardness. This could be attributed to a higher dislocation density due to processing condition D4 compared to C2 at the same load. In addition, although C2 laser processing resulted in lower hardness it showed lower dependence of hardness on depth when compared to D4.

Figure 21b-f depict load versus penetration depth for different processing conditions and for the as-received material at a load below 500 mN. The unloading curve for each plot is evidence of the extent of elastic recovery for each processing conditions. The highest elastic recovery was found in CTM302 (Figure 21e), followed by C2 and D4 (Figure 21c-b). This is evidence that shortest pulse duration and higher laser irradiances favour elastic recovery, on the other hand, longer pulse duration and lower energy densities (Figure 21d-f) might cause a reduction of elastic recovery in the material and consequently plastic deformation.

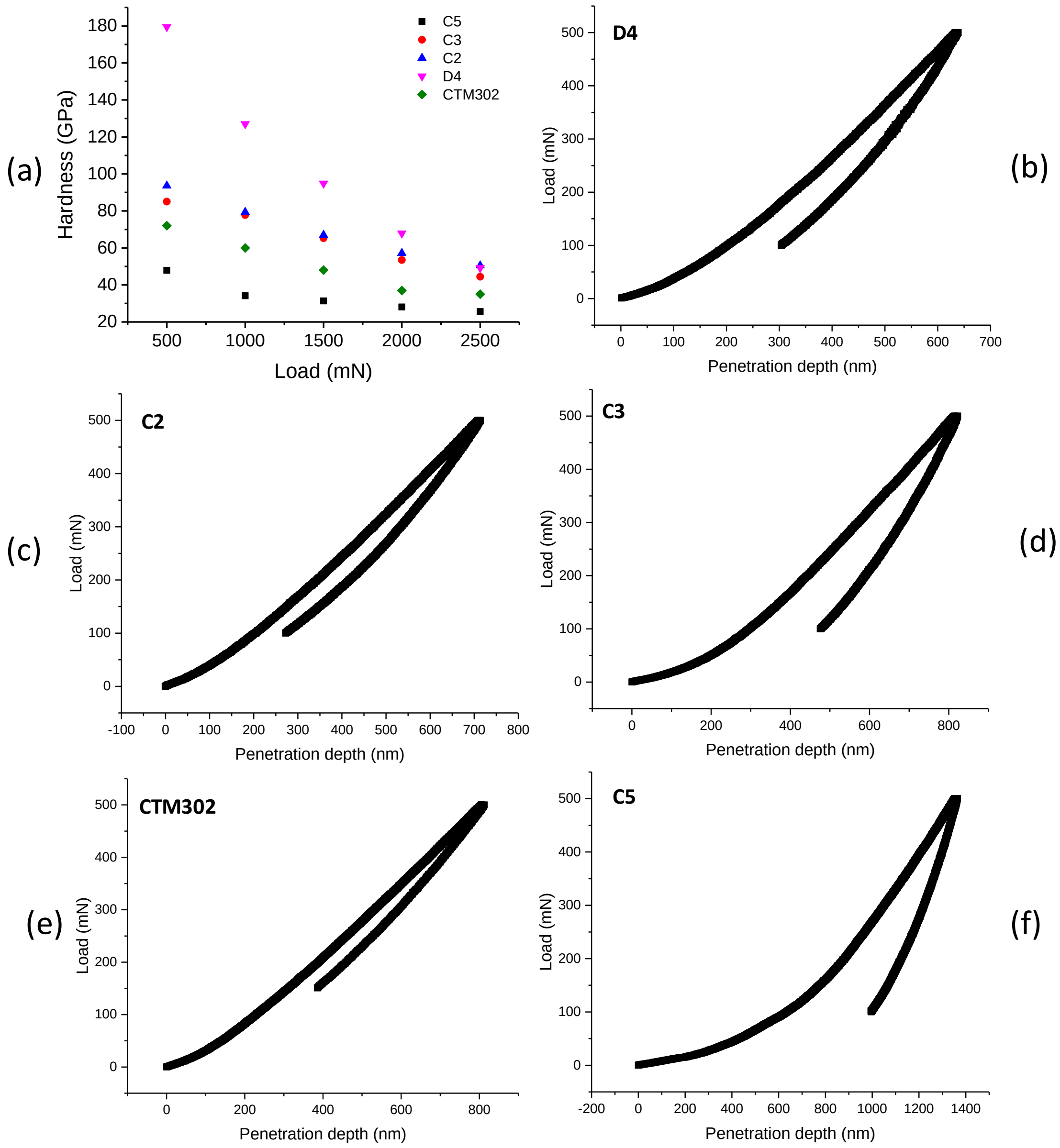

Figure 21: a) Load versus hardness for different materials, b-f) Load versus penetration depth for conditions: D4, C2, C3, CTM302, C5.

A previous study by Deng and Molian (2012) showed the effect of laser shock wave treatment on a polycrystalline diamond tool (grain size of 10 µm and 10% of cobalt binder volume) in relation to laser induced phase transition and hardness change. The main claim was that pulse repetition rate is more sensitive than peak power density in producing a change of hardness, due to an increase in dislocation density. At the same time, an increase in roughness was also reported. The results presented in this paper agree with the effect of pulse repetition rate suggested in the research by Deng and Molian (2012), however using a laser to excite thermally the polycrystalline structure just below its ablation threshold, a microstructural change accompanied by an increase in hardness and good surface integrity (140nm) were achieved.

4. Conclusions

Laser milling conditions were proposed to investigate the viability of fibre lasers for micro-engineering ultra-hard materials. An investigation of the effect of different thermal conditions on materials properties (e.g. hardness, micro-structure and metal binder volume) was presented. A step towards the fundamental understanding of the effects of variation of binder volume in the complex thermal and mechanical processes which underpin the laser machining of microstructurally different polycrystalline diamonds was made. For a fluence value of 11.34 J cm^{-2} (laser intensity of 0.052 GWcm^{-2}) in the nanosecond pulse regime, the two micro-structurally different PCD materials exhibit distinct milling mechanisms. SEM/EDX analysis revealed that for the heavier in diamond structure (CTM302) the thermal milling mechanism was dominated by Cobalt melting, ejection, and agglomeration at the grain boundaries without any conversion of diamond into graphite or amorphous carbon. While for the lighter in diamond structure (CTB010) a change in milling mechanism was noticed at different feed speed regions. This was found to be because of a recoil pressure which pushed the instantaneously converted amorphous carbon/graphite at the side of the grooves simultaneously with ejected Cobalt, later solidified (Figure 22).

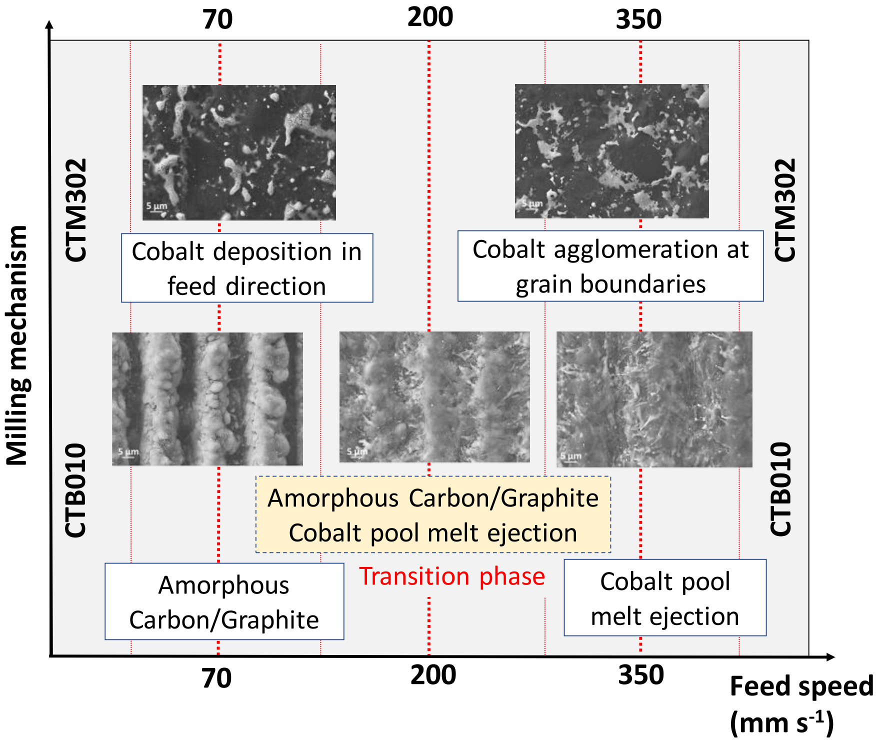

Figure 22: A schematic of the change in milling mechanism for the two microstructurally different materials.

Overall, the fundamental difference in the milled pockets of CTB010 and CTM302 at the same energetic conditions revealed that the main differentiating factor in the two polycrystalline structures is the presence of mechanical forces of different extent. CTB010 and CTM302 differ in grain size and grain distribution, the local positioning of the diamond grains increases the local strength, therefore CTM302 materials exercise higher local strength. In addition to this, the higher binder volume in CTB010 introduces loss of bonding between diamond's grains. A laser irradiance below the energy threshold can also enhance the surface integrity with a minimum roughness of 540 nm achieved for CTB010 and 140 nm for the multi-modal CTM302 which was revealed by topographical analyses. The achieved roughness is comparable to 50-100nm, measured on the as-received specimens. The thermal processing is highly affected by the metallic binder content, the lower the volume of metallic binder and the better surface roughness achievable. Micro-hardness measurements revealed that, specific milling conditions just below the material laser energy threshold can increase hardness (200-240 GPa) for high feed speed conditions up to a depth of 1 µm; SEM analyses also confirmed that the increased hardness up to 95GPa was accompanied by compressed grains, evidenced by striations on the crystallites. The strengthening effect on the microstructure might be due to the combination of heat treatment and plastic deformation of the crystallites. The probable change in diamond's grain size also affected dislocation movement, hence, by reducing the crystallite size more grain boundaries were formed which impeded dislocation movements and affected yield strength.

This study suggests that using a laser to thermally excite the polycrystalline structure just below its ablation threshold a change in microstructure and an increase in hardness can be achieved. The presented findings open new future perspectives in the utilisation of nanosecond fibre lasers to modify polycrystalline materials microstructure, enabling lasers to be embedded in the polycrystalline diamond material design.

Acknowledgment

The authors would like to acknowledge the support of Element Six Ltd. for providing the polycrystalline diamond materials.

References

Bitelli, G., Simone, A., Girardi, F., Lantieri, C., (2012). Laser scanning on road pavements: A new approach for characterizing surface texture, Sensors, 12 (7), 9110-9128.

Brecher, C., Klocke, F., Schindler, F., Janssen, A., Fischer, B., Hermani, J. P., (2013). Finishing of polycrystalline diamond tools by combining laser ablation with grinding, Produc. Eng., 7(4), 361–371.

Butler-Smith, P. W., Axinte, D., Pacella, M., Fay, M.W., (2013). Micro/nanometric investigations of the effects of laser ablation in the generation of micro-tools from solid CVD diamond structures, J. Mater. Process. Tech., 213, 194–200.

Chen, X. and Wang, H. X., (2001). A calculation model for the evaporation recoil pressure in laser material processing, Journal of Physics D: App. Phy., 34 (17), 2637–2642.

Christensen, B., Vestentoft, K., Balling, P., (2007). Short-pulse ablation rates and the two-temperature model, App. Sur. Sci., 253(15), 6347–6352.

Cook, M. W., Bossom, P. K., (2000). Trends and recent developments in the material manufacture and cutting tool application of polycrystalline diamond and polycrystalline cubic boron nitride, Int. J. Ref. Met. Hard Mat., 18, 147–152.

Dahotre, N. B., Harimkar, S., (2008). Laser fabrication and machining of materials, Springer, 248-250.

Deng, C., Molian, P., (2012). Laser shock wave treatment of polycrystalline diamond tool and nanodiamond powder compact, Int. J. Adv. Manu. Tech., 63 (1–4), 259–267.

Dold, C., Henerichs, M., Bochmann, L., Wegener, K., (2012). Comparison of Ground and Laser Machined Polycrystalline Diamond (PCD) Tools in Cutting Carbon Fiber Reinforced Plastics (CFRP) for Aircraft Structures., Proc. CIRP, 1, 178–183.

Dold, C., Henerichs, M., Gilgen, P., Wegener, K., (2013). Laser processing of coarse grain polycrystalline diamond (PCD) cutting tool inserts using picosecond laser pulses., Phys. Proc. Elsevier, 41, 610–616.

Haag, F., Beitelschmidt, D., Eckert, J., Durst, K., (2014). Influences of residual stresses on the serrated flow in bulk metallic glass under elastostatic four-point bending - A nanoindentation and atomic force microscopy study, Acta Mater., 70, 188–197.

Hall, E. O. (1951). The deformation and ageing of mild steel. III. Discussion of results. Proc. Phys. Soc. Lond. B 64, 747-753.

Hoffman, J. (2015). The effect of recoil pressure in the ablation of polycrystalline graphite by a nanosecond laser pulse, J. of Phys. D: App. Phys. IOP Publishing, 48, 235201.

Huang, Q., Yu, D. Xu, B., Hu, W., Ma, Y., Wang, Y., Zhao, Z., Wen, B., He, J., Liu, Z., Tian, Y., (2014). Nanotwinned diamond with unprecedented hardness and stability. Nature 510, 250–253.

Kidalov, S. V., Shakhov, F. M., (2009). Thermal Conductivity of Diamond Composites, Mater., 2(4), 2467–2495.

Lemaitre, J. (1985). A Continuous Damage Mechanics Model for Ductile Fracture, J. Eng. Mater. Tech., 107(1), 83–89.

Miess, D. and Rai, G. (1996). Fracture toughness and thermal resistance of polycrystalline diamond compacts, Mater. Sci. and Eng. A, 209(1–2), 270–276.

Ochsner, A. and Holm, A. (2016). Machining, Joining and Modifications of Advanced Materials. Springer.

Pacella, M., Butler-Smith, P. W., Axinte, D. A., Fay, M. W., (2014). FIB/TEM/EELS micro/nanometric investigations of the effects of laser ablation on the diamond/binder structure in polycrystalline diamond composites, J. Mater. Process. Tech., 214 (5), 1153–1161.

Pacella, M., Axinte, D. A., Butler-Smith, P. W. (2014). On the Topographical/Chemical Analysis of Polycrystalline Diamond Pulsed Laser Ablated Surfaces, Proc. CIRP 13, 387–392.

Pacella, M., Axinte, D. A., Butler-Smith, P. W., Shipway, P., Daine, M., Wort, C., (2015). An assessment of the wear characteristics of microcutting arrays produced from polycrystalline diamond and cubic boron nitride composites, J. of Manu. Sci. and Eng., 138 (2), p. 21001.

Petch, N. J. (1953). The cleavage strength of polycrystals. J. Iron Steel Inst. 174, 25-28.

Shukla, P., Smith, G. C., Waugh, D. G., Lawrence, J., (2015). Development in laser peening of advanced ceramics, Proc. SPIE, 9657, 96570.

Sun, X., Zhou, W., Kikuchi, K., Nomura, N., Kawasaki, A., Doi, H., Tsutsumi, Y., Hanawa, T., (2017). Fabrication and Characterization of a Low Magnetic Zr-1Mo Alloy by Powder Bed Fusion Using a Fiber Laser, Metals, 7(11), 501.

Tao, Q., Wei, X., Lian, M., Wang, H., Wang, X., Dong, S., Cui, T., Zhu, P., (2017). Nanotwinned diamond synthesized from multicore carbon onion. Carbon N. Y. 120, 405–410.

Tasan, C., Hoefnagels, J. P. M., Geers, M. G. D., (2009). Indentation based damage quantification methodology revisited, Proc. of 7th Euromech Solid Mech. Conf., 1–3.

Thoe, T. B., Aspinwall, D.K., Wise, M.L.H., Oxley, I.A., (1996). Polycrystalline diamond edge quality and and surface integrity following electrical discharge grinding, J. Mater. Process. Tech., 56(1–4), 773–785.

Vasantgadkar, N. A., Bhandarkar, U. V., Joshi, S. S., (2010). A finite element model to predict the ablation depth in pulsed laser ablation, Thin Solid Films, 519, 1421-1430.

Wu, Q., Wang, J., Huang, C., (2014). Analysis of the machining performance and surface integrity in laser milling of polycrystalline diamonds, Proceedings of the Institution of Mechanical Engineers Part B, J. of Eng. Manu., 228(6), 903–917.

Yan, M. T., Fang, G. R., Liu, Y. T. (2013). An experimental study on micro wire-EDM of polycrystalline diamond using a novel pulse generator, Int. J. of Adv. Manu. Tech., 66(9–12), pp. 1633–1640.

Yudasaka, M, Komatsu, T., Ichihashi, T., Achiba, Y., Iijima, S., (1998). Pressure Dependence of the Structures of Carbonaceous Deposits Formed by Laser Ablation on Targets Composed of Carbon, Nickel, and Cobalt, The J. of Phys. Chem. B, 102(25), 4892–4896.

Zaitsev, A. M., (2001). Optical Properties of Diamond: A Data Handbook. Berlin/Hei.

List of figures

Figure 23: SEM micrographs before machining of a) CTB010 and b) CTM302.

Figure 24: Abbott curve for one as-received surface and parameters Sk, Spk, Svk for two microscopically different materials.

Figure 25: Effect of feed speed on 2D surface roughness parameters for the two microscopically different materials.

Figure 26: Effect of feed speed on 3D texture parameters for the two microscopically different materials.

Figure 27: SEM images of CTB010 laser milled surfaces at different feed speeds: a) 70 mm s^{-1} (Ra = 4.3µm), b) 210 mm s^{-1} (Ra = 1.6µm), c) 350 mm s^{-1} (Ra = 1.4µm).

Figure 28: SEM images of CTM302 laser milled surfaces at different feed speeds: a) 70 mm s^{-1} (Ra = 0.5µm), b) 210 mm s^{-1} (Ra = 0.41µm), c) 350 mm s^{-1} (Ra = 0.31µm).

Figure 29: Effect of track distance at different spot overlaps and its influence on surface roughness parameters in CTB010 and CTM302.

Figure 30 Plot of spot overlap variation and its effect on surface roughness parameters in CTB010 and CTM302.

Figure 31: SEM images of CTM302: a) as-received sample, b) milled at 0.57 mJ in condition C5, c) milled at 0.57 mJ in condition C4. Details of the conditions can be found in Table 4.

Figure 32: Effect of increased number of passes for CTM302 (TD = 20µm, doc = 1µm): a) 1 pass (condition D5), b) 5 passes (condition C2), c) magnified detail of striations in one of the crystallites.

Figure 33: Alicona 3D images and Abbott curve for one surface of CTM302 (a, b) and CTB010 (c, d) milled surfaces at τ = 220 ns, ψ = 11.34 J cm^{-2}, I= 100%, FS = 1000 mm s^{-1}, TD = 20 µm, N=1, doc = 1 µm.

Figure 34: A schematic of the milling mechanism for the two microstructurally different materials at the same conditions: I = 100%, τ = 220 ns, ψ = 11.34 J cm^{-2}, TD = 20 µm, N=1, doc = 5 µm.

Figure 35: Topographical profile of CTB010 milled surfaces at I= 100%, FS = 1000 mm s^{-1}.

Figure 36: Abbott curve for one surface and parameters Sk, Spk, Svk of CTB010 milled surfaces at I= 100% and FS = 1000 mm s^{-1}.

Figure 37: Abbott curve for a single profile and the parameters Sk, Spk and Svk of CTM302 milled at I 100%, FS 1000 mms^{-1}.

Figure 38: SEM micrographs of CTM302 milled surfaces.

Figure 39: Surface roughness profiles of CTB010 and CTM302 (FS 1000 mms^{-1}, ψ = 11.34 J cm^{-2}, τ = 220 ns, TD = 28 µm) at: I = 80% (a, b); I = 100% (c, d).

Figure 40: Measurements of 2D roughness parameters extracted from Abbott-Firestone's curves at different processing conditions.

Figure 41: Graph of average measured valued of micro-hardness at a load of 500 mN in different processing conditions for CTM302 (CTM represents the the as-received sample).

List of Tables